Nucleic Acids Research, 2026, **54**, gkaf1443
https://doi.org/10.1093/nar/gkaf1443
RNA and RNA-protein complexes

Division of labor in trypanosome RNA processing and export through expanded Mex67 paralogs

Samson O. Obado[1,2,*], Peter C. Fridy[2], Eva Hegedűsová[3], Trevor van Eeuwen[2], Milana E. Stein[2], Wenzhu Zhang[4], Bryan C. Jensen[1], Connor Chung[1], Marc Brillantes[2], Lucy Glover[5], Zdeněk Paris[3], Brian T. Chait[4], Mark C. Field[3,6], Michael P. Rout[2,*]

[1]Center for Global Infectious Disease Research, Seattle Children's Research Institute, Seattle, WA 98101, United States
[2]Laboratory of Cellular and Structural Biology, The Rockefeller University, 1230 York Avenue, New York, NY 10065, United States
[3]Institute of Parasitology, Biology Centre, Czech Academy of Sciences, Branišovská 1160/31, 370 05, České Budějovice, Czech Republic
[4]Laboratory of Mass Spectrometry and Gaseous Ion Chemistry, The Rockefeller University, 1230 York Avenue, New York, NY 10065, United States
[5]Trypanosome Molecular Biology Unit, Institut Pasteur, Université Paris Cite, INSERM U1347, 25-28 Rue du Dr Roux, 75015, Paris, France
[6]School of Life Sciences, University of Dundee, Dow Street, Dundee, DD1 5EH, United Kingdom

*To whom correspondence should be addressed. Email: Obado@seattlechildrens.org
Correspondence may also be addressed to Michael P. Rout. Email: rout@rockefeller.edu

Abstract

In animals and fungi, bulk messenger RNA (mRNA) export to the cytoplasm is mediated by the Mex67/Mtr2 (NXF1/NXT1) heterodimer and driven by an ATP-dependent remodeling machinery on the cytoplasmic side of nuclear pore complexes, the exclusive gateways of nucleocytoplasmic transport. Uniquely, we show that trypanosomes have three distinct Mex67 paralogs (TbMex67, TbMex67b, and TbMex67L); each having a different non-redundant role in ribosomal RNA (rRNA) processing and mRNA export. Specifically, TbMex67 and TbMex67b retain canonical roles in mRNA export, albeit associating with specific mRNA cohorts and differing protein and mRNA interactomes in the vertebrate host and insect vector forms of the parasite. Further, TbMex67 and TbMex67b paralogs associate with the GTPase Ran export machinery, rather than ATP-dependent helicases, demonstrating significant departure in RNA export mechanisms in trypanosomes. In contrast, TbMex67L is not involved in mRNA export but primarily associates with ribosome biogenesis factors. Thus, in trypanosomes Mex67 paralogs have diverse functionalities with implications for evolutionary origins and diversity of the control of gene expression.

Graphical abstract

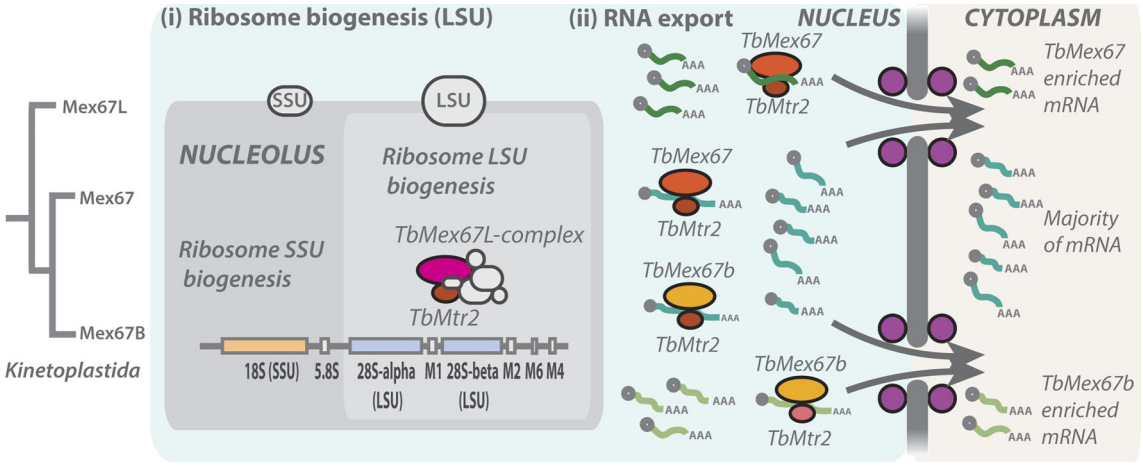

Introduction

Regulation of gene expression is a complex and highly dynamic process that extends from transcription to export progressing through a highly coordinated pathway involving numerous protein complexes. Significantly, multiple core mechanisms are shared across the tree of life, reflecting ancient ori-

Received: August 7, 2023. **Revised:** November 24, 2025. **Accepted:** November 25, 2025

gins. Multiple regulatory layers are exercised through modification of chromatin states, activation and repression of *cis*-acting elements and, through splicing, regulatory 5′ and 3′-untranslated regions (UTRs), translational efficiency and RNA degradation [1–4].

Numerous proteins associate with newly transcribed messenger RNAs (mRNAs) to form messenger ribonucleoprotein complexes (mRNPs). RNA export is coupled to transcription and processing, and closely integrated together forming transcription-export (TREX) complexes [5]. As RNA polymerase II transcribes mRNA, the THO/TREX complex, which includes the ATP-dependent RNA helicase Sub2 (UAP56 in animals), function as adaptors for other mRNA export proteins. THO/TREX mediates transcriptional elongation in yeast, remodels RNA, recruits the spliceosome, and aids in splicing of mRNAs in animals and co-transcriptional recruitment of mRNA export machinery in multiple eukaryotic lineages [6]. Beyond animals, fungi and plants the evolutionary and functional conservation of THO/TREX complex proteins are obscure, and no clear homologs have been identified with the exception of conserved Sub2 (UAP56) [5, 7–9]. Proteomics analysis of mRNA processing has highlighted involvement of both conserved and lineage-specific proteins in divergent lineages and specifically trypanosomes [10]. In all eukaryotes, mRNAs are exported to the cytoplasm via nuclear pore complexes (NPCs) prior to translation [11–13].

Nuclear export is mediated by transport factors that interact with phenylalanine–glycine (FG) dipeptide-rich proteins (FG–Nucleoporins or FG–Nups) that line the central channel of the NPC and provide a selectivity filter for nucleocytoplasmic transport. There are two major transport factor classes: karyopherins (importins and exportins) characterized by HEAT repeats [14], and nuclear transport factor 2 (NTF2) type factors which include the heterodimeric Mex67:Mtr2 (NXF1:NXT1 in animals) proteins that are major exporters of mRNA [15]. Directionality of most nucleocytoplasmic transport is provided by a RanGTP/GDP gradient which mediates assembly/disassembly of karyopherin-mediated transport complexes [16]. Significantly, the bulk mRNA export in animals, fungi and plants mediated by Mex67:Mtr2 and is an ATP-dependent and Ran-independent process. Specifically the ATP-dependent DEAD box RNA helicase Dbp5 (DDX19 in animals), and Gle1, associate with cytoplasmic-facing FG–Nup159 to remodel ribonucleoproteins (mRNPs) exiting the NPC [17–24]. Dissociation of the Mex67:Mtr2 complex, provides both directionality and the energy for mRNA export [25].

Nearly all understanding of NPC organization and gene regulation is derived from animals and fungi, both members of the opisthokont supergroup [26, 27]. Considerably less is known for other eukaryotic lineages, but significant evidence suggests mechanistic divergence in RNA export [28–31]. Trypanosomatids represent one of the most distant relatives of animals/fungi and possess noncanonical transcription mechanisms. Unlike most eukaryotes they lack individual gene specific RNA polymerase II (Pol II) promoters and instead co-transcribe multiple unrelated genes together in polycistronic transcription units (PTUs) [32]. Sequence specific Pol II promoters initiate transcription of PTUs while histone variants and modifications have also been shown to play a role in transcription start and termination sites of each PTU [33, 34]. mRNA stability is a key component of gene regulation in trypanosomes [35], but the mechanisms of mRNA export and processing remain poorly characterized, although recent efforts to identify key players have shown promise [10, 28, 29, 36]. Trypanosomes appear to lack the canonical surveillance systems preventing defective or unspliced mRNA from exiting the nucleus, which intriguingly aggregate within cytoplasmic mRNP granules proximal to the NPC [37].

Mex67, Mtr2, and karyopherins are evolutionarily conserved in trypanosomes [38–42]. Silencing TbMex67 or TbMtr2 strongly inhibits poly(A) RNA export, supporting its role as a *bona fide* mRNA export factor [38]. TbMex67 and TbMtr2 have additional roles in the export of transfer RNA (tRNA) [43] and pre-ribosomal subunits [44, 45], also conserved functions with animals and fungi [46–49].

In common with opisthokonts, TbMex67 (Tb927.11.2370) interacts directly with the Mtr2 ortholog, and together interact with the NPC [29, 38]. Surprisingly, TbMex67/TbMtr2 also interacts with Ran, Ran-binding protein 1 (RBP1) and a GTPase-activating protein (GAP) [29], a significant distinction from opisthokont Mex67 that relies on the RNA helicase Dbp5 to release mRNA cargo and is unable to bind Ran [50, 51]. *In silico* modeling suggests that interaction between TbMex67 and TbMtr2 with Ran is likely to be indirect [29]. Additionally, there is considerable divergence between the cytoplasm mRNA export platform of the trypanosome and higher eukaryote NPCs that reflect mechanistic differences in the energetics of mRNA export [28, 29]. Specifically, trypanosome NPCs lack the canonical components of the opisthokont cytoplasmic mRNA Nup159/Gle1/Dbp5 remodeling platform (Nup214/Gle1/DDX19 in humans) [17, 52, 53], but instead possess two large cytoplasmic FG–Nups (TbNup140 and TbNup149), of which TbNup149 has several putative zinc finger motifs with no equivalents in opisthokont NPCs [8, 28, 29, 41]. Furthermore, additional NPC/NE features such as a divergent nuclear basket, a noncanonical lamina, and unique mRNA decapping complexes, indicate significant mechanistic divergence [9, 54–57]. There is also evidence that Sub2 and other mRNA processing factors include lineage specific proteins [10].

We now demonstrate here that trypanosomatids possess a specialized RNA export system encompassing multiple Mex67 paralogs. One TbMex67 paralog, TbMex67L, associates with a rRNA biogenesis complex, indicating a distinct mechanism and potential evolutionary pathway for the coordination of export of multiple RNA classes. We propose a new model for the evolution of RNA processing and nuclear export in trypanosomatids, highlighting unique solutions to RNA export selected by different eukaryotic lineages.

Materials and methods

Cell culture

Trypanosoma brucei procyclic form (PCF) Lister 427 strain cells were cultured in SDM-79, supplemented with 10% fetal bovine serum as previously described [41]. Expression of plasmid constructs was maintained using hygromycin B at 30 μg/ml. *T. brucei* bloodstream form (BSF) 427 cells were cultured in HMI-9T a modification of the original IMDM-based HMI-9 [58] that uses 56 μM 1-thioglycerol instead of 200 μM 2-mercaptoethanol, 2 mM glutaMAX I (Invitrogen) instead of 4 mM l-glutamine, and supplemented with 10% fetal bovine serum (non-heat inactivated in our case) as previously described [59]. Expression of plasmid constructs in this life stage was maintained using hygromycin B at 3 μg/ml.

In situ genomic tagging

All protein-coding sequences were tagged using the pMOTag4G tagging vectors [60] as previously described [29, 41].

Phylogenetic analysis of the TbMex67 paralogs

Mex67 orthologs were retrieved by interactive BLAST from the NCBI dataset downloaded locally and searched using custom scripts [61]. Sequences were aligned using MUSCLE [62] and trimmed using alncut from the FAST suite [63], and a phylogeny calculated using FastTree2 [64].

Fluorescence microscopy and RNA fluorescence in situ hybridization (RNA FISH)

GFP-tagged cell lines were harvested and fixed for 10 mins in a final concentration of 2% paraformaldehyde. Fixed cells were then washed in 1× phosphate buffered saline (1 x PBS), and visualized as previously described [29]. RNA FISH was performed as previously described [43]. Briefly, 1×10^7 cells were harvested and washed with PBS. Cells were resuspended in 4% paraformaldehyde/PBS solution and fixed to poly-L-lysine coated microscope slides for 30 min and dehydrated using an increasing gradient of ethanol concentrations (50%, 80%, and 100%, for 3 min each). Permeabilized cells were pre-hybridized with hybridization solution (2% bovine serum albumin (BSA), 5× Denhardt's solution, 4× saline-sodium citrate (SSC), 5% dextran sulfate, 35% deionized formamide, and 10 U/ml RNase inhibitor), for 2 h, then incubated overnight at room temperature in a humid chamber in the presence of 10 ng/μl Cy3-labeled oligonucleotide probes in hybridization solution. Slides were then washed for 10 min, once with 4× SSC with 35% deionized formamide, then one wash each with 2× SSC and 1× SSC. Finally, the slides were mounted with mounting medium supplemented with 4′,6-diamino-2-phenylindole dihydrochloride (DAPI). Images were taken with confocal microscope Olympus FluoView™ FV1000 and analyzed using Fluoview and ImageJ (NIH) software. FISH data were quantified as described previously [43].

Affinity isolation and purification of TbMex67 paralog protein interactome

Affinity capture of the TbMex67 paralogs was performed as previously described [29]. Briefly, Insect stage procyclic (PCF) trypanosomes were grown to a density of between 2.5×10^7 cells per ml, and BSF parasites were grown to a density of 2.0×10^6 cells per ml. Parasites were harvested by centrifugation, washed in 1× PBS (plus 20 mM glucose for BSFs), with protease inhibitors and 10 mM dithiothreitol, and flash frozen in liquid nitrogen to preserve protein–protein interactions as close as they were at time of freezing as possible. Cells were cryomilled into a fine grindate in a planetary ball mill (Retsch). For a very detailed protocol, refer to our methods paper [65], or the National Center for Dynamic Interactome Research website (www.NCDIR.org/protocols). Cryomilled cellular materials were resuspended extraction buffers (20 mM HEPES, 250 mM NaCl, 10 μM $MgCl_2$, and 0.5% Triton for TbMex67 and TbMex67b; 20 mM HEPES, 20 mM NaCl, 50 mM tri-sodium citrate, 10 μM $MgCl_2$, and 0.5% Triton for TbMex67L), containing a protease inhibitor cocktail without EDTA (Roche), and clarified by centrifugation ($20\,000 \times g$) for 10 min at 4°C [29, 65]. Clarified lysates were incubated with magnetic beads conjugated with polyclonal anti-GFP llama antibodies on a rotator for 1 h at 4°C. The magnetic beads were harvested by magnetization (Dynal) and washed three times with extraction buffer prior to elution with 2% sodium dodecyl sulfate (SDS)/40 mM Tris pH 8.0 for protein. Eluates were fractionated using sodium dodecyl sulfate - polyacrylamide gel electrophoresis (SDS–PAGE) on NuPAGE™ 4%–12% Bis Tris gels (Invitrogen) and stained using GelCode™ Blue Stain (Thermo Scientific).

Identification of protein–protein interactions by mass spectrometry

Briefly, eluates from affinity capture experiments were loaded into the wells of a 5% acrylamide gel and run at 100 V for ∼5 min to allow the proteins to migrate ∼2 mm into the gel. The gels were then fixed for 5 min in 50% methanol/7% acetic acid and then stained using GelCode™ Blue Stain (Thermo Scientific). The resultant protein bands from each well were excised from acrylamide gels as a gel plug and destained using 50% acetonitrile, 40% water, and 10% ammonium bicarbonate (v/v/w). Gel pieces were dried and resuspended in trypsin digestion buffer; 50 mM ammonium bicarbonate, pH 7.5, 10% acetonitrile, and 0.1–2 μg sequence-grade trypsin, depending on protein band intensity. Digestion was carried out at 37°C for 6 h prior to peptide extraction using C_{18} beads (POROS) in 2% TFA (trifluoroacetic acid), and 5% formamide. Extracted peptides were washed in 0.1% acetic acid (ESI) and analyzed on a LTQ Velos (ESI) (Thermo). ESI LC-MS data were analyzed using the Global Proteome Machine [66]. Identified proteins were ranked by peptide log intensity and the top 50 hits selected for further analyses.

Affinity isolation and purification of TbMex67 paralog RNA cargo

Affinity capture was performed as described above, with the modifications. We maximized RNA yield using ultrafast affinity capture using our very high affinity double nanobody with a K_d of 36 pM [67]. This allowed us to complete affinity isolation experiments in 10 min, minimizing degradation, and spurious nonspecific interaction issues. RNA was extracted from these isolations using the Trizol and Zymo Research Direct-zol RNA extraction Kit. Magnetic beads were incubated with Trizol for 10 min and RNA extracted using the manufacturer's protocols (Zymo Research). Extraction buffer for RNA associated with TbMex67 and TbMex67b was 20 mM HEPES, 150 mM NaCl, 10 μM $MgCl_2$, and 0.5% Triton for RNA extraction. For TbMex67L, the extraction buffer was 20 mM HEPES, 20 mM NaCl, 50 mM tri-sodium citrate, and 0.5% Triton. We also tested stabilization of the TbMex67 complexes using glutaraldehyde, which was added to our affinity capture buffer for 5 min and quenched using Tris, pH 8.0, prior to resuspending the frozen cell grindate. We tested RNA-Seq using both glutaraldehyde-stabilized and nonfixed samples and observed no significant differences in RNA identified, and proceeded with the nonfixed samples for further experiments (data not shown). We utilized Agilent RNA Pico chips to ensure the integrity and enrichment of RNA under various buffer conditions on small-scale purifications. Extracted RNA was sequenced using The Rockefeller University Genomic Center Illumina HiSeq 2000. Given the highly dynamic nature of RNA export, we performed 75 bp paired end sequencing for each affinity captured RNA cargo (three biological replicate experiments for TbMex67 and Tb-

Mex67b and two for TbMex67L) without poly(A) RNA enrichment or rRNA depletion because of well documented observations that opisthokont Mex67/Mtr2 (NXF1/NXT1) interacts with both rRNA and mRNA (reviewed in [68], as does TbMex67 which has been shown to be involved in the export of tRNA [43] and pre-ribosomal subunits [44, 45]. RNA-Seq reads were aligned using HISAT2 v2.2.1 [69] to the *T. brucei* 927 reference genome, or the 2018 427 genome for VSG genes. Reads were quantified using featureCounts v2.0.3 [70] and differential enrichment was analyzed with edgeR v3.36.0 [71], with $P = 0.01$ used as a cut-off. Counts are reported as fragments per kilobase of transcript per million mapped reads (FPKM). GO enrichment analysis was performed on TbMex67- or TbMex67b-enriched transcripts using the PANTHER Overrepresentation Test (Released 20 240 807), with *T. brucei* GO biological processes (GO Ontology database DOI: 10.5281/zenodo.16423886), using a 5% false discovery rate cut-off.

RNA interference and loss of function tests

RNA interference (RNAi) was performed using the 2T1 (BSFs) and PT1 (PCFs) cell lines [72]. Briefly, 1 kb segments from each TbMex67 paralog was polymerase chain reaction (PCR) amplified from *T. brucei* genomic DNA and cloned into the pRPa^{iSL} plasmid and transfected into 2T1 BSFs and PT1 PCFs. Cells were grown to a density of 2×10^7 ml^{-1} and induced using 1 μg ml^{-1} of tetracycline. Additional cell lines were generated using the RNAi 29–13 cells [73] to test RNAi efficiency for the TbMex67, TbMex67b, and TbMex67L in PCFs.

CRISPR knockout of TbMex67b and TbMex67L in procyclics

Guide RNAs (gRNAs) were designed from http://grna.ctegd.uga.edu/. Criteria for chosen gRNAs were based off a GC content close to 50% and were within ∼50 bp from TbMex67b and TbMex67L. 0.5 μl (32 pmol) of Alt-R™ L.b. Cas12a (Cpf1) Ultra (idtdna.com) was combined with 2 flanking guide RNAs (as close to translation start and end, also from IDT, resuspended in 10 mM Tris, 0.1 mM EDTA pH 7.5 to 32 μM) each at a final 16 pmol (0.5 μl each) to a final volume of 10 μl with 10 mM Tris, 0.1 mM EDTA pH 7.5. Cas12a and gRNAs were combined and incubated at RT for 10 min. Primers (not containing gRNA sequence) to TbMex67b and TbMex67L UTRs were used to PCR a KO cassette (pSM07, containing puromycin resistance). The KO cassette (∼ >6 μg in this case) along with the entire Cas12/gRNA reaction was added to the resuspended cells in a 2 mm cuvette. Cells were electroporated using the Amaxa Nucleofector II (X-001) and resuspended in media not containing the selectable marker. Cells were immediately plated into a 96-well plate and puromycin was added after 8 h for selection of resistant cells. After selection, clones were screened for double KO via gDNA isolation and PCR screen using both external and internal primers to the gene open reading frame (ORF) to confirm proper integration of cassette and deletion of gene.

Secondary structure prediction, and structural modeling

The secondary structures of all three TbMex67 paralogs were predicted by HHPred [74]. Predictions of TbMex67 paralogs and their interaction with TbMtr2 were generated using AlphaFold2 [75]. For potentially greater accuracy, a Discoba taxon specific database was used for multiple sequence alignments [76]. A modified version of AlphaPickle [M. J. Arnold. 2021. AlphaPickle. doi.org/10.5281/zenodo.5708709.] was used to generate the predicted error of alignment (PAE) plots and structural predictions were visualized in ChimeraX [77].

Results

TbMtr2 associates with the trypanosome NPC and the ran machinery

We *in situ* GFP-tagged TbMtr2 and performed affinity capture and identified interaction partners by liquid chromatography mass spectrometry (LC-MS). Under stabilizing conditions, TbMtr2 affinity captured the entire NPC (Fig. 1A), similar to TbMex67, as we previously demonstrated [29]. However, using more stringent affinity isolation conditions, a smaller subset of NPC nucleoporins (TbNups) (Fig. 1A) were identified, including the TbNup76 complex (TbNup76, 140, and 149) as we previously demonstrated for TbMex67 [29], consistent with a conserved role for this complex in RNA export [28, 29]. TbMtr2 also associates with components of the outer ring complex (TbNup89, 132, and 158). These connections with the TbNup76 complex and the outer ring likely reflect conserved NPC interactions also found in animals and fungi where the mRNA export platform (ScNup82/HsNup88 complexes) is tethered to the NPC by outer ring components [52]. Significantly, as we have previously shown for TbMex67 [29], TbMtr2 also co-purified with an entire Ran GTPase cycle apparatus; Ran, Ran-binding protein 1 (RanBP1), and a TBC-domain-containing GTPase-activating protein (TbGAP, Gene ID Tb927.10.7680, which was previously termed TBC-Root_A [78]) (Fig. 1A). TbGAP possesses a Rab-GAP type TBC-domain and is present within a TBC-domain protein phylogeny root but significantly is absent from animals and fungi [78]. A close evolutionary relationship between Ran and Rab GTPases may indicate that all originally utilized a TBC-domain GAPs, but which has been replaced/diverged in animals and fungi so that the TBC domain is absent from Ran GAP proteins. Another intriguing property of the TbGAP is the presence of an N-terminal UBA domain similar to that of NXF1 separated from the TBC domain by a disordered central domain [28]. This is rather unusual because opisthokont RanGAPs typically have several LRR domains [79], which is lacking in this putative RanGAP [28].

Trypanosomatids possess three Mex67 paralogs

Surprisingly, TbMtr2 not only interacts with TbMex67 (confirming interaction with TbMex67 [29, 38]) but also with two additional proteins, Tb927.11.2340 (58 kDa) and Tb927.10.2060 (108 kDa). We designate these TbMex67b and TbMex67L (for TbMex67-Like) respectively, as both interact with TbMtr2 and contain characteristic LRR and NTF2-like domains, major architectural features of Mex67 [80, 81] (Fig. 1B). TbMex67 possesses a CCCH-type Zn^{2+} finger, a feature thus unique to trypanosome Mex67 orthologs, differentiating them from animal, fungi, and plants. Significantly, the Zn^{2+} finger domain is essential for TbMex67 to function as an mRNA export factor [38, 40, 82]. TbMex67 possesses a C-terminal ubiquitin-associated domain (UBA) (Fig. 1B and C), conserved with yeast Mex67/metazoan NXF1 and required in those, for FG–Nup binding [83]. By contrast

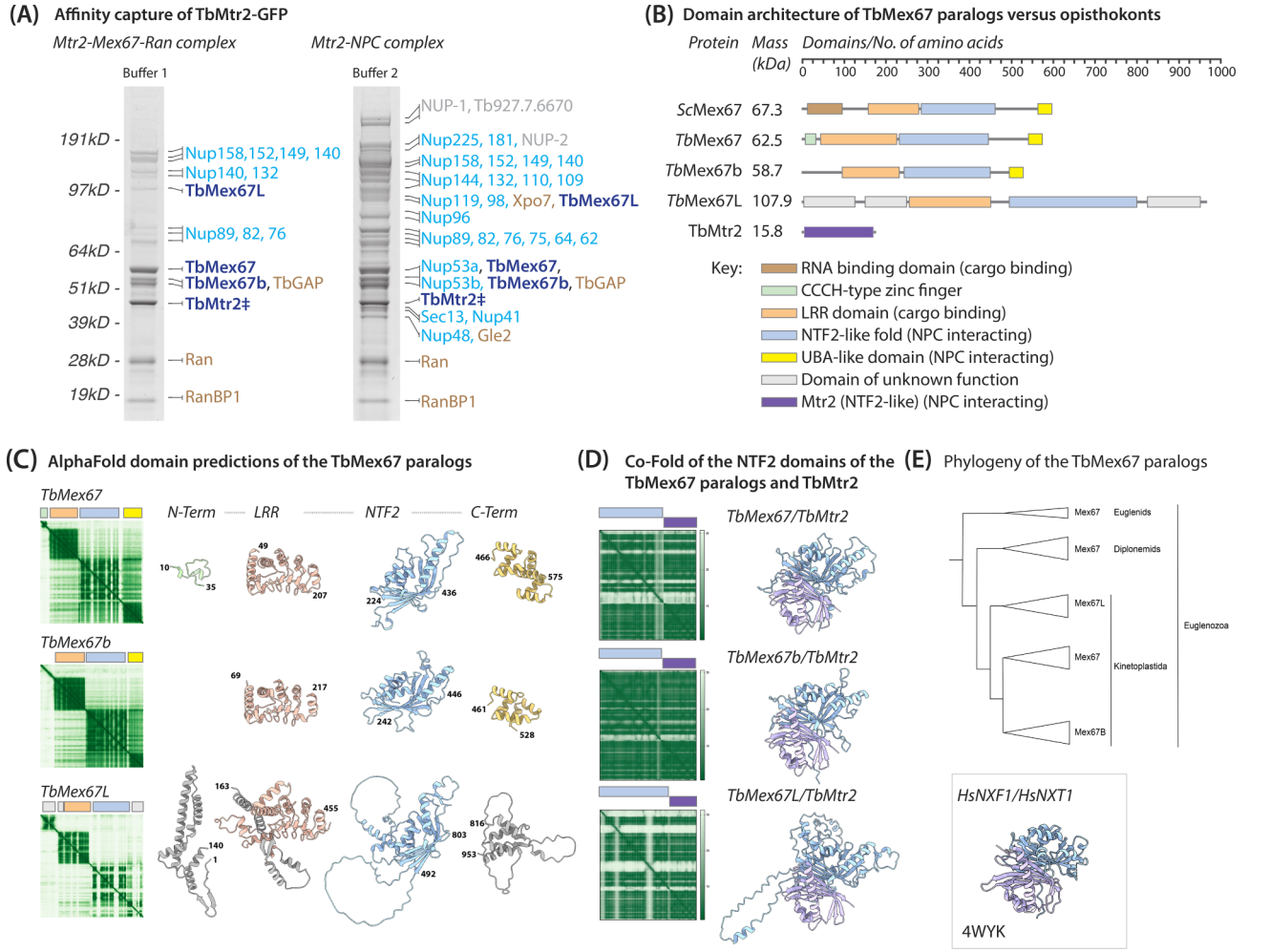

Figure 1. Affinity capture of the TbMtr2 and identification of new Mex67 paralogs. (**A**) Using the GFP tagged TbMtr2 (marked with a ‡), under high stringency biochemical conditions (Buffer 1), we affinity isolated structural components of the NPC (sky blue), transport factors connected to the GTPase Ran cycle (orange), and TbMex67 (navy blue) with which TbMtr2 is known to form a heterodimer (38). In addition, we discovered interaction with two putative TbMex67 paralogs which we termed TbMex67b and TbMex67L (for like or large) denoted in navy blue like TbMex67. Under low stringency conditions (Buffer 2), we affinity isolated the entire trypanosome NPC as well as exportin 7 (Xpo7), the RNA export component Gle2 (85–87) and the lamin proteins NUP-1 and NUP-2 (54 133), and a hypothetical protein (gray). Affinity isolates were resolved by SDS–PAGE and visualized by Coomassie staining. Proteins bands were excised and identified by mass spectrometry. (**B**) A schematic of the domains that are present on each protein and highlights the difference between them. (**C**) An illustration of the differences between the architecture and domains of the three TbMex67 paralogs as predicted by AlphaFold (76). The confidence scores (green) for each TbMex67 paralog has been scaled to the same size for ease of illustration. (**D**) Co-folding of the NTF2 domains of each individual TbMex67 paralog with TbMtr2 and comparing the resulting heterodimer with the crystalized structure of human NXF1:NXT1, (84) showing high functional homology and suggesting that all three TbMex67 paralogs are *bona fide* Mex67/NXF1 orthologs. The confidence scores (green) for each TbMex67 paralog has been scaled to the same size for ease of illustration. (**E**) A phylogenetic tree showing the distribution of the TbMex67 paralogs within Euglenozoa.

TbMex67b lacks the Zn^{2+} finger but retains the LRR, NTF2-like and UBA domains (Fig. 1B and C). TbMex67L is more divergent from TbMex67/TbMex67b and is significantly larger. TbMex67L contains the LRR and NTF2-like domains, but lacks the C-terminal UBA domain, and instead possesses an extended N-terminus characterized by coiled coils and a C-terminal region, both of unknown function, together with unstructured loops within the NTF2 domain (Fig. 1B and C) [75, 76].

Thus, all three trypanosome Mex67 paralogs possess NTF2 domains required for interaction with Mtr2. We used AlphaFold to perform *in silico* co-folding of the NTF2 domains of each paralog with TbMtr2, which predicted their interactions as similar to the experimentally characterized interaction interface between the human NTF2-like domain of NXF1 and NXT1 [84] (Fig. 1D). Although based on homology modelling, this supports our affinity capture protein–protein interaction data suggesting that TbMtr2 is an adaptor for all three TbMex67 paralogs, and that all are bonafide Mex67 paralogs. Interestingly, multicellular organisms such as humans which have additional tissue specific variants of NXF1 that form heterodimers with NXT1 or NXT2 although these are not as divergent from each other as the trypanosome Mex67 paralogs [80].

TbMex67b and TbMex67L are kinetoplastid specific

The genes encoding TbMex67 and TbMex67b are 5 kb apart on chromosome 11, suggestive of an origin through a lineage-specific gene duplication event. Indeed, the chromosomal environment, including the synteny of these and surrounding

genes, is conserved throughout the kinetoplastids. Phylogenetic reconstruction across all kinetoplastids indicates that TbMex67 and TbMex67b are much more closely related than they are to TbMex67L, as expected from such a duplication event (Fig. 1E and Supplementary Fig. S1 for the full phylogenetic tree). Significantly, orthologs of TbMex67 and TbMex67b are recovered from all kinetoplastid genomes, including the free-living bodonid, *Bodo saltans*, indicating that the duplication predates the origin of parasitic trypanosomatids. Interestingly, Mex67L is absent from the *B. saltans* genome, *albeit* retained within all other kinetoplastids, suggesting a more recent origin.

TbMex67 paralogs are differentially localized

The divergence in trypanosome Mex67 paralog architecture suggests these proteins may support distinct functions. We *in situ* GFP-tagged each paralog in both procyclic (PCFs, insect stage) and BSFs (vertebrate stage) and determined cellular location by fluorescence microscopy (Fig. 2A). Similarly to TbMtr2, both TbMex67 and TbMex67b strongly localize to the nuclear envelope in puncta characteristic of nucleoporins, many nuclear transport factors, and other NPC-associated proteins [41], in both life stages (Fig. 2A). Further both TbMex67 and TbMex67b partly localize to the nucleoplasm and the nucleolus (Fig. 2A), as previously described for TbMex67 [39]; these similarities suggest related functional roles. By contrast TbMex67L has a localization distinct from TbMex67 and TbMex67b, and is nucleolar, with no discernable nuclear peripheral staining in either life stage, suggestive of a unique function compared to TbMex67 or TbMex67b (Fig. 2A).

TbMex67 paralogs have distinct protein–protein interactomes

Affinity isolations of TbMex67 and TbMex67b co-purified similar protein cohorts with an interesting distinction (Fig. 2B and Supplementary Table S1). Both associate with Mtr2 and the same subset of nucleoporins that interact with TbMtr2 (Fig. 1A). We suggest that TbMex67 and TbMex67b interact at the NPC largely through three FG–Nups (TbNups 140, 149, and 158) and indirectly with TbNup76, which is attached to the outer ring [29]; however given their function as transport factors, they likely associate with other FG-repeat containing Nups. This association with Nups is consistent with the localization of both paralogs to the NPC at the nuclear periphery and likely represents proteins in transit as they ferry cargo across (Fig. 2A). TbMex67 and TbMex67b also associate with members of the Ran GTPase system, confirming that TbMex67b likely functions as a nuclear transporter as previously shown for TbMex67 by us [29].

In addition to Nups and the Ran system, TbMex67 and TbMex67b also co-purify with TbGle2 (ortholog of yeast Gle2 or Rae1 in animals [85–87]), as well as poly(A) binding protein 2 (PABP2) (Fig. 2B and Supplementary Table S1 for extended interactome) in PCFs. Trypanosomes have two poly(A) binding proteins, PABP1 and PABP2, that differ in intracellular localization and distribution on polysome fractionation under conditions that disrupt mRNA metabolism [88]. Only PABP2 accumulates in the nucleus when mRNA export is disrupted, and appears to be associated with bulk mRNA compared with PABP1 that associates with a smaller cohort of mRNAs [89]. PABP2 has been shown to be involved in the control of mRNA stability and processing through stabilization of the poly(A) tail [90]. In contrast to TbMex67 in BSFs, the TbMex67b interactome includes PABP2, the ATP-dependent RNA helicase TbSub2 (UAP56 in animals), and HYP, a protein of unknown function termed HYP [10] (Fig. 2B and Supplementary Table S1). Enrichment of PABP2, Sub2 and HYP with TbMex67b over TbMex67 suggests both have discrete functional roles in BSFs. Notably, this distinction between TbMex67b and TbMex67 is not unique to *T. brucei* as affinity isolation experiments performed using *T. cruzi* Sub2 copurifies with HYP and the *T. cruzi* Mex67b ortholog but not the *T. cruzi* Mex67 as observed by us for *T. brucei* [10]. TbMex67b was also noted as a protein of unknown function that together with a cohort of proteins associates DRBD18 in BSFs [91]. It has also been shown that TbMtr2 and TbMex67 associate with an abundant RNA-binding protein DRBD1, which mediates selective export of certain mRNAs in PCFs [92].

Interestingly, TbMex67L also interacts with Mtr2 (Figs 1A and 2B), explaining its affinity capture using TbMtr2 as an affinity handle. Beyond this, there is essentially no concordance between the TbMex67L and TbMex67/TbMex67b interactomes, and a large subset of nucleolar-associated proteins implicated in ribosomal biogenesis (Fig. 2A and Supplementary Table S1). Amongst these, the nucleolar protein NOP168 is trypanosome specific [93], while NOG1 is a widely conserved nucleolar GTPase [93], that coordinates ribosome formation [94]. NOP89, also nucleolar localized [93], is required for synthesis of 28S and 5.8S ribosomal RNAs (rRNAs) and thus the large ribosome subunit [95]. Significantly, no nucleoporins or transport factors were identified even though it partners with TbMtr2, but consistent with an absence from the nuclear periphery and significantly, the absence of the UBA domain required for NPC association at the C-terminus of Mex67L [96, 97]. Collectively, both location and protein–protein interactions indicate a role in ribosomal biogenesis, and suggest that TbMex67L disengages from maturing ribosomal subcomplexes prior to engagement with the NPC and export machinery [25, 47–49, 51, 80, 98, 99].

All TbMex67 paralogs are essential and nonredundant

We used RNAi to test for essentiality and functional redundancy between the three TbMex67 paralogs. RNAi mediated depletion of each paralog resulted in severe loss of fitness in BSFs, suggesting essentiality (Fig. 3). TbMex67 has been shown to be essential in PCFs [38, 43, 44], and our RNAi result recapitulates this observation (Fig. 3). RNAi silencing of TbMex67b resulted in no clear phenotype, whilst that of TbMex67L resulted in a gradual loss of fitness over several cell cycles in PCFs, as observed in a global RNAi screen of all *T. brucei* genes [72]. A significant difference in RNAi efficiency between the BSF cell lines versus the PCF cell lines was tested by quantitative PCR using telomerase reverse transcriptase (TERT) RNA as a control. Knockdown efficiency was 84%, 67%, and 55% in BSFs and 68%, 5%, and 22% in PCFs for TbMex67, TbMex67b, and TbMex67L, respectively, across three clonal replicates. Despite testing multiple new cell lines, the RNAi silencing efficiency for TbMex67b and TbMex67L in PCFs remained poor and in some cases, there was a slight increase in TbMex67b mRNA, making the interpretation of any phenotype difficult. We noted similar observations for TbMex67b in a global RNAi screen in which

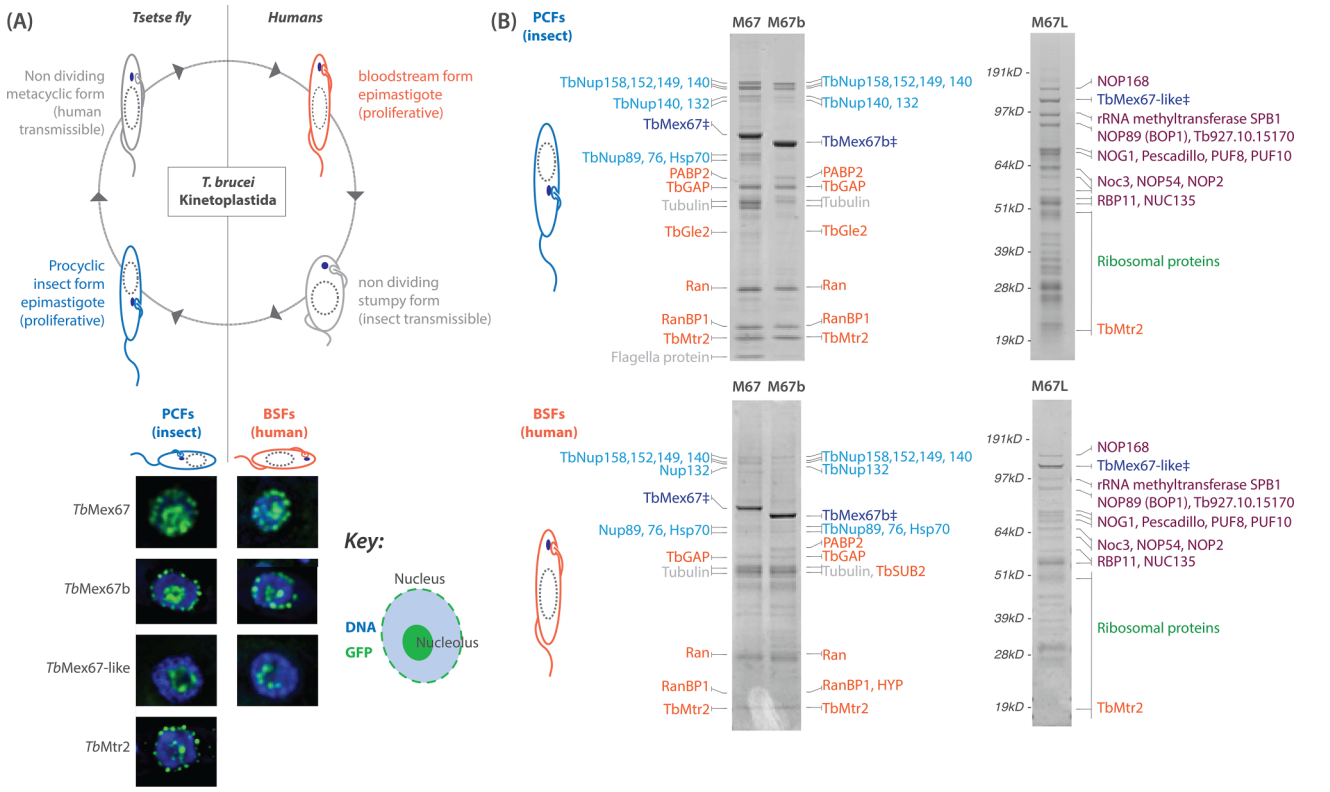

Figure 2. GFP tagging of the TbMex67 paralogs and their protein interactomes. (**A**) We *in situ* GFP tagged TbMex67, TbMex67b, and TbMex67L at their chromosomal loci in both the PCFs that infect tsetse flies and the BSFs that infect vertebrates. The TbMtr2-GFP from PCFs is shown for comparison. We found that except for TbMex67L, other paralogs and TbMtr2 localize to NPCs at the nuclear envelope as well as the nucleoplasm albeit predominantly around the nucleolus. (**B**) We performed affinity capture using each GFP tagged paralog in PCFs and BSFs (marked with a ‡) and discovered that TbMex67 and TbMex67b interact predominantly with the NPC, whilst TbMex67L interacts only with ribosome biogenesis proteins, possibly a reflection of its nucleolar only localization. However, there is a significant difference between the interactomes of TbMex67 and TbMex67b in BSFs, with TbMex67b forming additional interactions with TbSub2, HYP, and PABP2, suggesting it may operate in a pathway that distinguishes it from TbMex67 in BSFs.

there's a similar increase in RNA counts for TbMex67b in the trypanosome genome database (TriTrypDB) [72]. We therefore decided to attempt a double knockout (trypanosomes are diploid) of the TbMex67b and TbMex67L genes in PCFs where the RNAi phenotype led to a slow gradual loss of fitness (TbMex67L) or resulted in no significant loss of fitness (TbMex67b) (Fig. 3). We discovered that we could easily knockout both alleles of TbMex67b in PCFs using a CRISPR–Cas12 system (see Materials and methods). However, the resultant TbMex67b null cells (ΔTbMex7b) have a significant growth phenotype and divide at half the rate (2.3× per day) of wild-type cells (4.1× per day) (Supplementary Fig. S2). These findings suggest that despite being nonessential for survival in axenic culture, TbMex67b contributes critically to PCFs, with its function only partially offset by compensatory pathways. Regarding TbMex67L, despite multiple rounds of transfections, we were only able to generate single knockout cells (TbMex67L-SKO), suggesting that TbMex67L is essential in PCFs (Supplementary Fig. S2). This supposition is supported by the observation that TbMex67L-SKO divide at 3.2× per day compared to wild-type cells (4.1× per day).

TbMex67 and TbMex67b, but not TbMex67L, are required for RNA export

We used poly(A) FISH (fluorescence *in situ* hybridization) to probe for a role in export of polyadenylated RNA. RNAi silencing of TbMex67 in BSFs and PCFs led to accumulation of the poly(A) RNA signal in the nucleus and depletion from the cytoplasm (Fig. 3), as previously observed in PCFs [38, 43, 44]. Interestingly, RNAi mediated depletion of TbMex67b in BSFs led to poly(A) RNA accumulation in the nucleus and around the nuclear periphery (Fig. 3), suggestive of a role in RNA processing and export. The accumulation of poly(A) around the nucleus is reminiscent of nuclear periphery granules that occur as a result of unspliced mRNA being exported out of the nucleus but remain tethered to the NPC [37]. Association of TbMex67b and TbSub2 hints at the possibility that Mex67b may function in conjunction with the trypanosome equivalent of the THO/TREX complex [6]. These data likely reflect a continuum of mRNP export intermediates, encompassing an early Sub2 dependent loading step and later NPC-associated export states. We are investigating this further. In PCFs, we performed RNAi FISH on the RNAi cell lines despite low RNAi efficiency (above) and on the ΔTbMex7b cell lines. We did not observe poly(A) accumulation in the nuclei of either cell lines suggesting that TbMex67b may have a different functional role in PCFs versus BSFs. The caveat is that we have likely selected ΔTbMex7b mutant cells adapted to survive in axenic culture using unknown compensatory mechanisms. Nonetheless, in conjunction with localization and protein interacting partners, these data suggest that TbMex67 and TbMex67b are independently required for mRNA export in BSFs. In PCFs, TbMex67 is the major exporter of mRNA and is essential to

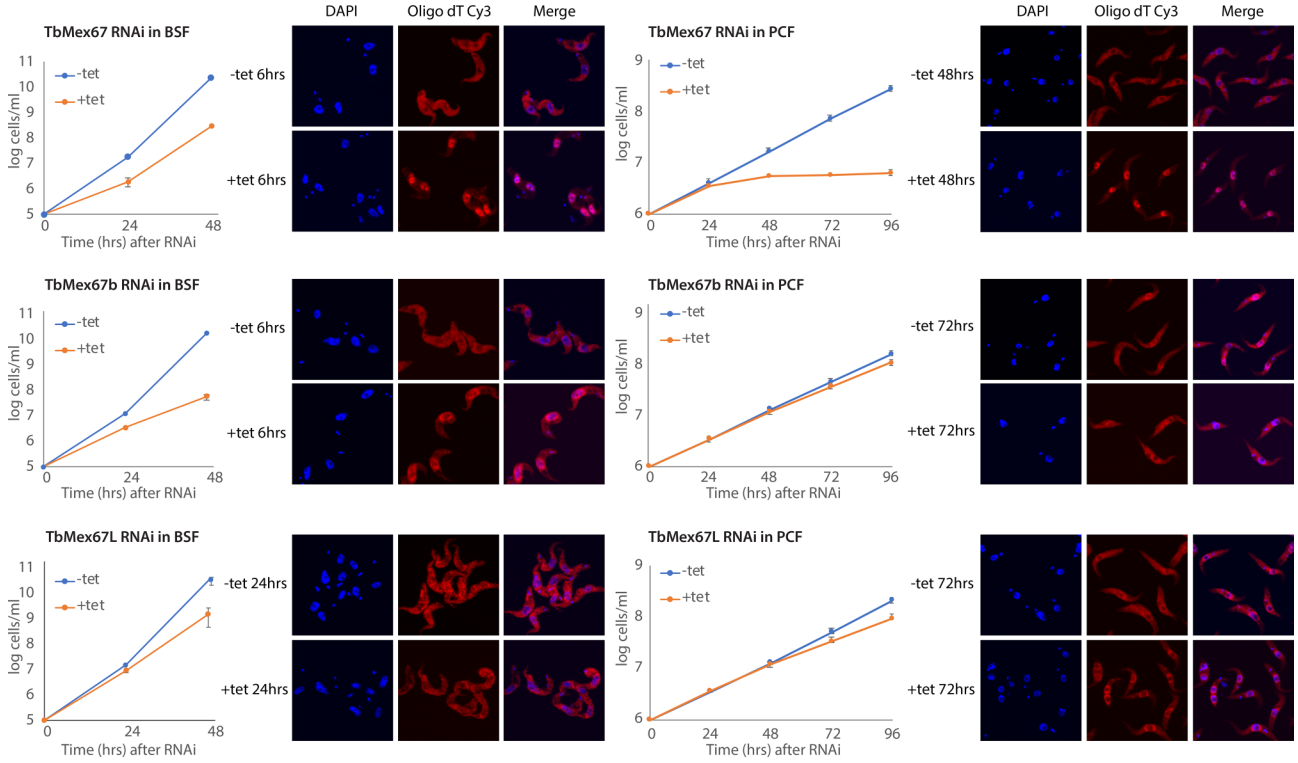

Figure 3. RNA interference knockdown of the Mex67 paralogs and poly(A) FISH to determine role in RNA export. To assess the role of the TbMex67 paralogs on mRNA export, we performed RNA FISH after induction of RNAi silencing for each individual paralog. There was a rapid loss of fitness in BSFs, accompanied by accumulation of mRNA in the nucleus of TbMex67, and in and around the nuclei of TbMex67b cell lines, but not TbMex67L indicating it is not involved in mRNA export. In PCFs, there was a rapid loss of fitness in TbMex67 cell lines post RNAi induction and accumulation of mRNA in the nucleus, but not in the TbMex67b cell lines which are less affected by RNAi ablation of the TbMex67b RNA. The RNAi KD is extremely poor (5%) in these cell lines. RNAi loss of fitness was very gradual post RNAi induction in TbMex67L cell lines. However, unlike in BSFs, over time, there is a gradual halo-like mRNA accumulation around the nuclei of the TbMex67L cell line. We are investigating TbMex67b and TbMex67L further.

the cell as previously shown [38, 43, 44], and recapitulated in this work. TbMex67b has similar localization as TbMex67 in PCFs, and associates with NPC components, transport factors, in addition to TbGle2 and PABP2 just like TbMex67 (Fig. 2). These associations and localization point to a putative role in nuclear transport since they share similar interactomes. Based on our assays, TbMex67 is sufficient to compensate for the loss of TbMex67b in PCFs, albeit at significant cost in fitness of the parasite (Supplementary Fig. S2). Whether this partial level of compensation is sufficient for survival in physiological context (in the insect vector) is unknown.

There was no nuclear accumulation of mRNA in BSFs following the RNAi silencing TbMex67L, consistent with a nucleolar localization and protein interactome consisting of ribosome biogenesis components such as NOG1 that has been shown to be required for biogenesis of the 60S subunit in trypanosomes [100]. In PCFs, there appears to be a gradual accumulation of polyadenylated RNA at the edge of the nucleus at 72 h post RNAi (Fig. 3), that may be due to a secondary effect due to loss of ribosomal assembly and hence protein synthesis. These results suggest that TbMex67L does not have the canonical Mex67 role in mRNA nuclear export but instead functions at the level of ribosome biogenesis based on its protein interactome.

Differential RNA associations of TbMex67 paralogs

Several studies link TbMex67 to the export of mRNA, tRNA and rRNA in trypanosomes [38, 43, 44]. Thus, we decided to survey all types of RNA that may be associated with the three TbMex67 paralogs. We affinity isolated TbMex67 and TbMex67b from PCFs and BSFs under conditions ensuring maximal preservation of RNA–protein interactions, extracted associating RNA and performed RNA-Seq (Fig. 4, and Supplementary Fig. S3 and Supplementary Table S2). mRNA export is a highly dynamic and transient process. Therefore, when performing RNA Immunoprecipitation Sequencing (RIP-Seq), we expect to observe a snapshot of a multitude of RNA export events in that are dynamic and stochastic.

Upon affinity capture, isolation and sequencing of the resultant of RNA, we found that TbMex67 and TbMex67b both associate with a large cohort of mRNA species (Fig. 4A). While 65% of these are at similar abundance, differential enrichment analysis found statistically significant enrichment (P-value < 0.01) of subsets of mRNA species in TbMex67 and not TbMex67b and vice versa, in both PCFs and BSFs (Fig. 4A). We performed a GO term enrichment analysis with a false discovery rate of $<5\%$, to determine if there is a significant concordant difference between the isolated RNA species in the TbMex67 versus TbMex67b datasets (Supplementary Table S2). We observed statistically significant enrichment ($P < 0.01$) in mRNA-associated biological processes (e.g. transcription, export, and localization) for TbMex67 in both BSF and PCF forms, and metabolic processes, glycosylation and rRNA processing in TbMex67b (listed in Supplementary Table S2).

Looking more closely at transcript enrichment among this set of mRNA-associated genes, we found that Tb-

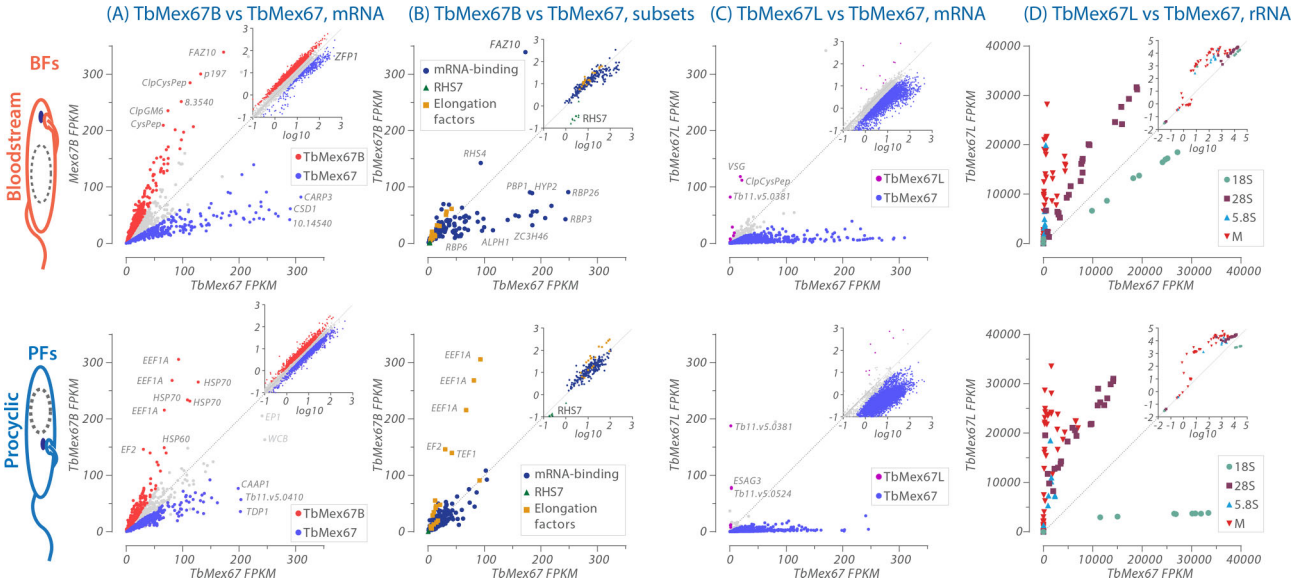

Figure 4. Affinity capture and identification of the RNA cargo of each TbMex67 paralogs. We affinity captured each TbMex67 paralog in PCFs and BSFs, then extracted interacting RNA and performed Illumina sequencing to determine which RNA species each paralog interacts with. Results were plotted on a linear scale (main graph), as well as in $\log_{10}$ (inset graph). In all the graphs, the *X*-axis represents TbMex67, which has been characterized in various studies, whilst the *Y*-axis represents either TbMex67b or TbMex67L, both of which had not yet been characterized prior to this study. The gray points on each graph represent transcripts that are not differentially enriched with statistical significance ($P > 0.01$). (**A**) TbMex67 (blue) and TbMex67b (red) share common mRNA cargo in both BSFs and PCFs, with a subset of mRNA species enriched in TbMex67 or TbMex67b, with highly abundant transcripts such as elongation factor 1-alpha (EEF1A) and heat shock protein (HSP70) in PCFs and calpain cysteine peptidase (ClpCysPep) in BSFs for TbMex67b. (**B**) There is a significant enrichment of mRNA encoding RBPs and zinc finger proteins on the BF TbMex67 mRNA cargo as compared with TbMex67b, suggesting a possible role in control of gene expression in this life cycle stage given the role of RBPs in the post transcriptional regulation of genes in trypanosomes (35). (**C**) As expected from its interactome, TbMex67L does not associate significantly with mRNA, as compared to TbMex67 (blue). Curiously the few mRNA species (purple) that associate with TbMex67L are the same in both BSFs and PCFs and are mainly pseudogenes of VSGs and ESAGs) (**D**) TbMex67L interacts primarily with rRNA cargo in both BSFs and PCFs as illustrated in a comparison between TbMex67 versus TbMex67L rRNA cargo, consistent with its nucleolar localization and its protein interactome that comprises several rRNA biogenesis factors. The TbMex67L rRNA interactome consists mainly of the components of the large (60S) subunit (5.8S and 28S), whilst 18S rRNA is enriched inTbMex67 rRNA cargo compared to TbMex67L. This 18S enrichment is more significant in PCFs compared to BSFs.

Mex67 has significant enrichment (*P*-value < 0.01) of zinc finger or RNA-binding proteins (RBPs) in BSFs (Fig. 4B), with ZFP1 (Tb927.6.3490), RBP26 (Tb927.7.3730), RPB3 (Tb927.11.530), and ZC3H46 (Tb927.11.16550) being among the most abundant mRNA species in this cohort, and enriched 2.7- to 8-fold over TbMex67b. ZC3H46 is involved in repression of gene expression [101], whilst ZFP1 is transiently enriched during differentiation [102]. RBP26 is amongst six mRNA transcripts upregulated following induction of RBP6, a master regulator of transformation of PCFs into infectious metacyclic forms, that also preferentially associates with TbMex67 over TbMex67b (Fig. 4B) [103, 104]. HYP2 mRNA also preferentially associates with TbMex67 over TbMex67b and is involved in signaling pathways involved in the formation of bloodstream "stumpy" parasites that are transmitted to tsetse flies [105]. This suggests that TbMex67 may be one of several proteins modulating developmental regulation in trypanosomes, in addition to exporting general mRNA cargo.

Additionally, mRNAs encoding PAB1-binding protein 1 (PBP1), the mRNA decapping enzyme ApaH-like phosphatase (ALPH1) [57] and retrotransposon hot spot protein 7 (RHS7) transcripts are significantly enriched in BSFs with the TbMex67 cohort compared to TbMex67b (Fig. 4B) (2- to 12-fold enrichment, *P*-value < 0.01). RHS protein genes are abundant and grouped into seven categories, with RHS2, 4 and 6 involved in transcription and translation [56]. The function of RHS7 is unknown and as such the significance of preferential association with TbMex67 is currently unclear. TbMex67b also has significant enrichment (3- to 8-fold enrichment, *P*-value < 0.01) of several high abundance elongation factor transcripts (elongation factor 1-α and elongation factor 2) in PCFs compared to TbMex67 (Fig. 4B).

Given the difference in essentiality of TbMex67 and TbMex67b in the two major life cycle stages we also examined transcripts of the major surface antigens, namely procyclins in PCFs and variant surface glycoproteins (VSGs) in BSFs (Supplementary Fig. S3) that are the major surface proteins in both life cycle stages [106–110], and are generated by Pol I transcription, a unique feature of the African trypanosome [111, 112]. Our hypothesis was that perhaps TbMex67b has a unique role in export of VSG transcripts since it is essential in the blood stage of the parasite, whilst TbMex67 is a general exporter because it is essential in all life cycle stages. However, at our sequencing resolution, both TbMex67 and TbMex67b associate with procylins and a dominant VSG transcript with no statistically significant enrichment. However, we noted that while the dominant VSG transcript showed no preference for TbMex67 or TbMex67b, TbMex67b showed a statistically significant depletion of other VSG transcripts relative to TbMex67 in both PCFs and BSFs, seen in both GO-term enrichment analysis and when comparing relative VSG transcript abundances (Supplementary Fig. S4, Supplementary Table S2, and Supplementary Table S3). The presence of multiple VSG transcripts associated with TbMex67 and TbMex67b paralogs is consistent with many earlier studies, and in par-

ticular evidence for multiple VSG mRNAs within the nucleus, but with few or just one VSG mRNA in the cytoplasm (Supplementary Figs S3 and S4) [113, 114]. This new evidence suggests that nascent transcripts associate with the Mex67 export machinery, but that the homotype VSG is by far the most abundant, and hence that the mechanisms preventing entry to the cytosol and translational machinery are pre-engagement with the Mex67 export apparatus *per se*, and hence may be associated with events at, or close to, the NPC. Given the proximity between the active VSG and the spliced leader locus at the ESB, it is tempting to speculate that "inactive-" VSG mRNAs lack a 5′-miniexon, and hence are marked for nuclear retention/degradation [115].

We also asked if UTR length or GC content of the isolated RNAs were biased towards TbMex67 and TbMex67b RNA cargos, and observed that transcripts enriched with TbMex67 had lower GC content (mean %GC of 43.1% versus 50.5% in BSF, 44.1% versus 47.9% in PCF) and longer 3′ UTRs (mean of 1280 versus 641 bp in BSF, 1114 versus 526 in PCF) than those enriched with TbMex67b ($P < 0.0001$ by Mann–Whitney test for all comparisons) (Supplementary Fig. S5). We are currently investigating the significance of these differences.

TbMex67L is required for the biogenesis of the 60S ribosomal subunit

We affinity captured TbMex67L, isolated the associated RNA and compared with that of TbMex67 (Fig. 4C and D) and TbMex67b (Supplementary Fig. S1). TbMex67L does not associate with mRNAs (Fig. 4C), apart from nineteen RNA Pol I transcripts that are mainly pseudogenes of VSGs and expression site associated genes (ESAGs). Curiously these few VSG pseudogenes and ESAGs are the same in both BSFs and PCFs and. There has previously been an interesting observation that TbMex67 prevents readthrough of Pol I transcription beyond chromosomal loci of procyclin genes [116], raising the possibility of a similar function forTbMex67L.

Consistent with a nucleolar localization and protein interactome enriched with ribosome biogenesis factors, we found that the affinity-isolated RNA associated with TbMex67L consisted of several rRNA transcripts (28S, 5.8S, and M1-6 rRNA [117]) that together form the pre60S subunit, indicating a role in large subunit assembly (Figs 2 and 4D). We tested the impact of TbMex67L RNAi and TbMex67 (as a control) in BSFs on ribosome biogenesis, choosing this life stage on account of the more rapid response of RNAi in comparison to PCFs to avoid pleiotropic effects. We harvested the RNAi-induced BSFs 18 hours post RNAi induction, lysed cells in the presence of cycloheximide and fractionated their polysomes over a sucrose gradient. Strikingly, RNAi ablation of Mex67L resulted in depletion of the 60S LSU peak, but not the 40S SSU peak. RNAi knockdown of TbMex67 did not affect the 40S or 60S peaks (Fig. 5A). This suggests that Mex67L is involved in the biogenesis of the LSU and not the SSU, and consistent with the presence of NOG1, a core protein in LSU biogenesis in the TbMex67L interactome [100].

Ribosome biogenesis primarily occurs in the nucleolus where RNA polymerase I synthesizes a large pre-rRNA (35S in yeast, 47S in humans), which contains the 18S rRNA and two of the three LSU rRNAs (25S and 5.8S in yeast, 28S and 5.8S in humans) [118, 119]. The rRNAs are typically flanked by so called external transcribed spacers (5′ ETS and 3′ ETS) and separated by internal transcribed spacers (ITS1 and ITS2). The rRNA precursor undergoes co-transcriptional folding, processing, and modification, enabling the initial assembly and maturation of both ribosomal subunits within the nucleolus and the nucleoplasm. Unlike in yeast and humans, the trypanosome LSU is segmented and processed as six fragments: two large fragments (LSUα and LSUβ), and four distinct small ribosomal rRNAs (sr1, 2, 4, and 6) (Fig. 5B), a hallmark feature not observed in other eukaryotes [119]. Thus, we reexamined our TbMex67L RIP-Seq data to test whether we observe intermediary pre-rRNA processing steps.

We discovered that the rRNA from the TbMex67L affinity captured large ribosomal subunit (LSU) are not yet fully processed and still contain internal transcribed spacers ITS2, ITS3, and ITS4 that interconnects both two large fragments (LSUα and LSUβ), as well as two of the four distinct small ribosomal rRNAs (sr1 and sr2) (Figs 5B and 5C). Interestingly, we were only able to affinity capture the LSU rRNA, with very little SSU rRNA in PCFs, unlike BSFs, which co-isolates both SSU and LSU (Fig. 5C). This observation could be a result of dynamics of processing as we do not observe ITS1 in 18S sequences from the BSF. However, it is consistent with the observed difference in enrichment of 18S sequences between the BSFs and PCFs (Fig. 4D). Concomitantly, TbMex67 and TbMex67b also associate with preferentially with 18S rRNA (Figs 2B and 4C). Interestingly, TbMex67 and TbMtr2 have been implicated as involved in ribosome biogenesis as loss of either leads to irregular rRNA processing and aberrant polysome and ribosome formation [44, 45, 82]. It is unclear if opisthokont Mex67/Mtr2 are involved in ribosome biogenesis, but they are associated with the export of both the 40S and 60S ribosomal subunits in yeast [47, 49].

Discussion

We have shown here that trypanosomatids have diversified an ancestral Mex67 into three paralogs that retain interaction with Mtr2 but support distinct cellular functions. All three share a core protein architecture and form heterodimers with Mtr2 likely via their evolutionarily conserved NTF2 domain and possess an LRR domain, but outside of the core, each paralog has distinct features. TbMex67 uniquely has an N-terminal CCCH zinc finger essential for function [38], while TbMex67 and TbMex67b both have C-terminal UBA domains (Fig. 1). TbMex67L is considerably larger than the other two paralogs, due to extensive N- and C-terminal regions. Furthermore, TbMex67L has a large predicted unstructured domain within the NTF2 domain (perhaps a reason that the TbMex67L/TbMtr2 does not interact with NPCs) and lacks the UBA-like domain important for mediating interactions with the THO complex component Hpr1 [83, 120] and the FG–Nups of the NPC [96]. Concomitantly, TbMex67L localizes to the nucleolus and lacks obvious mRNA export functions.

We conclude that TbMex67 and TbMex67b are both *bona fide* mRNA exporters as they localize and interact with the NPC, associate with mRNA and are required for mRNA export, albeit TbMex67b is dispensable in PCFs albeit with a significant growth phenotype. Although TbMex67 and TbMex67b in PCFs were not observed to associate stoichiometrically with many RBPs, we detected TbPABP2 and TbGle2 [41, 86] at substoichiometric levels by LC-MS, likely highlighting the dynamism of the system. Gle2 (Rae1 in animals) is associated with mRNA export as its perturbation leads to nuclear

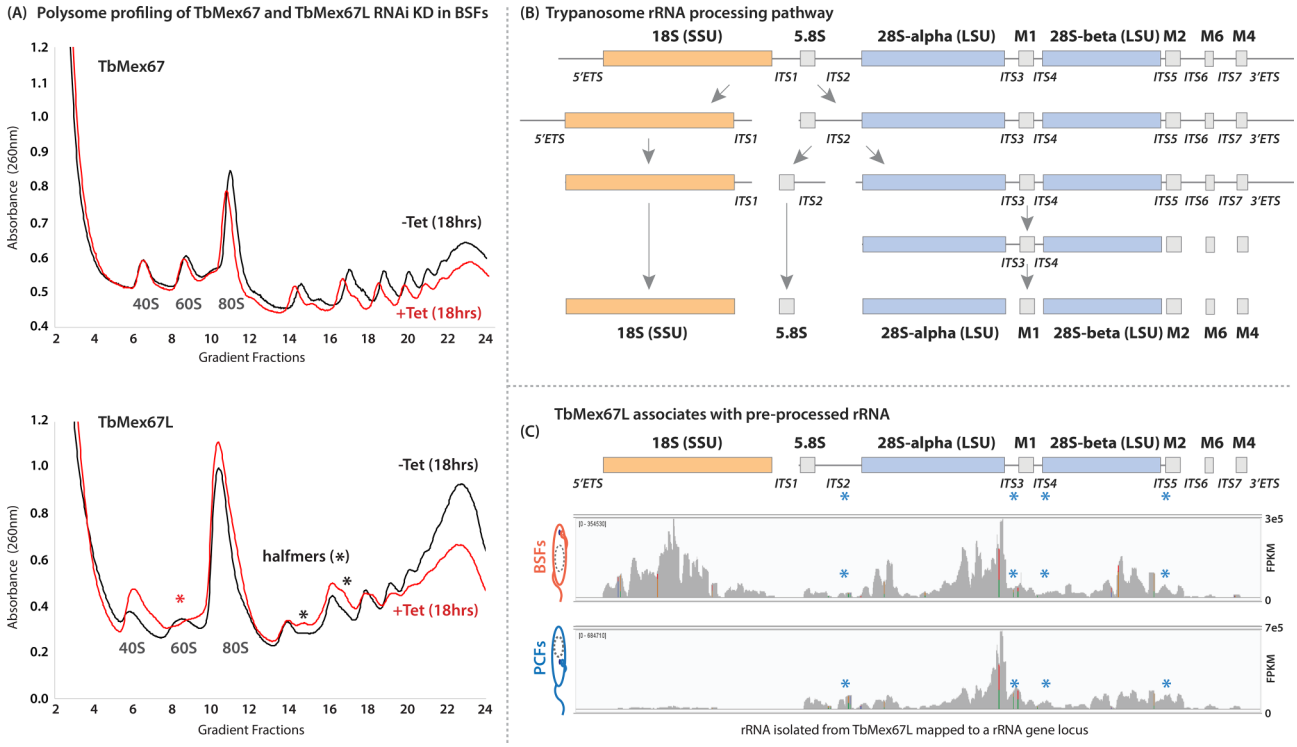

Figure 5. TbMex67L is involved in 60S (LSU) maturation. (**A**) Polysomes were prepared at 18hrs to avoid pleiotropic effects associated with dying cells, from Control (−Tet) and RNAi cells (+Tet) for TbMex67 and TbMex67L RNAi cell lines. RNAi KD of TbMex67L results in a drop in the 60S peak and the appearance of shoulders (halfmers) on the polysome profile of cells depleted of TbMex67L, but not TbMex67 showing that this phenotype is specific for TbMex67L. (**B**) A schematic of the trypanosome rRNA processing pathway. The 28S rRNA is fragmented into two large and four small fragments unlike in opisthokonts. (**C**) In both BSFs and PCFs affinity isolated RNA, the LSU is still connected to the 5.8S, M1, M2 as well as ITS2, 3, 4, and 5, suggesting TbMex67L associates with LSU rRNA that is still being processed. Additionally, there is an association of TbMex67L with SSU rRNA in BSFs parasites and not insect stage PCF parasites that is apparent in Fig. 4.

accumulation of poly(A) RNA in yeast and humans [87, 121]. There are two poly(A) binding proteins in trypanosomes; TbPABP1 and TbPABP2 that also differ in their interactions with very distinct cohorts of mRNAs as well, perhaps segregating associating *cis*-acting elements [88], and the two exporting TbMex67 paralogs could have a similar functional bias although this hypothesis is yet to be fully tested. Additionally, there is a clear contrast between the protein interactomes of TbMex67 and TbMex67b in BSFs. TbMex67b associates with TbSub2, and HYP, suggesting that the TbMex67 and TbMex67b may operate on two separate pathways, or—more speculatively—upstream and downstream of one another in RNA processing, considering that Sub2 is an integral component of the THO/TREX complex [6] (Fig. 2).

Interestingly, the *T. cruzi* Mex67b and HYP orthologs were recently identified in a proteomic screen using TcSub2 as the affinity handle, strongly supporting its role as being involved in mRNA export [10]. The recapitulation of this Mex67b-specific Sub2 and HYP interaction in *T. brucei* thus remains intriguing. On the other hand, TbMex67 has a significantly higher association with mRNAs encoding RBPs in BSFs (Fig. 4), suggestive of a role in gene regulation in this life cycle stage. This complex involvement of likely several RBPs with the TbMex67 paralogs shows that further analyses is required to delimit the roles of each paralog in BSFs and PCFs.

Several lines of evidence indicate that TbMex67L operates in rRNA maturation and ribosomal assembly rather than mRNA processing and export and disengages prior to ribosomal subunit export. This functional distinction is probably a comparatively newer adaptation in the evolution of eukaryotes as TbMex67L retains both the Mtr2-interacting domain and an interaction with Mtr2, which together form an obligate FG–Nup repeat interacting region in other Mex67 homologs. We speculate that TbMex67L may have retained weak interactions with FG repeats to allow a lower degree of FG–Nup association than we can currently detect, but sufficient enough to aid in import of the heterodimer into the nucleus so that it can access the nucleolus. This functional distinction is, to our knowledge, unique amongst Mex67 homologs [80]. It may also have revealed a previously suspected, but not dissected, direct role for Mex67 in RNA processing and assembly to generate a mature RNP in many eukaryotes—including ourselves—as well as its role normally in export of the mature RNP out of the nucleus [45].

It is well documented in opisthokonts that Mex67/NXF1 is also involved in the export of ribosomal subunits through the Crm1/XPO1–NMD3 pathway (reviewed in [68]). Similarly, TbMex67 participates in the NMD3 pathway in trypanosomes, suggesting a level of evolutionary conservation [44]. We suggest that TbMex67 and TbMex67b also have roles in 40S subunit export, as evidenced by their interaction with 18S rRNA. TbMex67 may also function in 60S export in trypanosomes via interaction with the 5S RNP [82].

While other unicellular lineages appear to possess just one Mex67 gene, metazoans can encode several isoforms of Mex67 or NXF, albeit closely related in sequence and structure (unlike TbMex67, TbMex67b, and TbMex67L) and some of which are generated as splice variants [80, 122–125].

For instance, vertebrates have six NXF gene products, namely NXF1–NXF6 [80]. NXF1 (Mex67) is found in all tissues and is considered the global conserved mRNA exporter in metazoa whilst NXF2, NXF3, and NXF5 have tissue specific functions in the testes or neurons [80, 125–127]. NXF5 localizes to neurons and associates with translating ribosomes, stress granules, and P-bodies [123, 126, 128–130]. NXF1 and NXF2 predominantly localize to the nucleoplasm and display mRNA export activities, whilst NXF3 and NXF5 are mainly cytoplasmic, highlighting possible functional differences [80, 131]. Importantly, NXF1, 2, and 3 form a heterodimer with NXT1 (Mtr2) which facilitates NPC localization and translocation [15, 25, 97, 122, 132].

Gene regulation is a core cellular process, and with the advent of eukaryogenesis the evolution of the nuclear brought new opportunities. Many of the processes that mediate selective mRNA expression are in part or wholly located at the nuclear envelope. Trypanosomes, one of the earliest groups to separate from the main eukaryotic lineage, can offer a glimpse into alternate mechanisms across cellular processes. Many studies have highlighted the distinct nature of the components supporting mRNA processing and frequently rationalized as a reflection of the use of *trans*-splicing mechanisms in the resolution of nascent mRNAs and the absence of differential *cis*-splicing. This means that, at the same time, there is potentially reduced burden in mRNA quality control but also an increased role for mRNA-based processes in terms of control of protein copy number. Here, we have shown that there are three Mex67 paralogs, each with a unique role, and also that there is association of these proteins with differentiation pathways and the mediation of transcriptional cascades. There is also a highly distinct mechanism at play as all three Mex67 proteins interact with the Ran system, further differentiating trypanosomes and other lineages. This ties in with current knowledge that the trypanosome NPC has a divergent architecture especially at the nuclear basket and cytoplasmic mRNA export platform [28, 29]. Furthermore, the Ran cycle is apparently mediated by a TBC GAP, significant as TBC GAPs in animals and fungi operate on Rab proteins with Ran GAP proteins bearing distinct architecture.

One interpretation is that the roles of Mex67 expanded in trypanosomes and switched to a Ran-mediated mechanism from an ATP-mediated one, but the alternative hypothesis, that trypanosomes would represent the ancestral state is also appealing. Here, there would have been a single mechanism that controls all nuclear export, regardless of the type of cargo, and the Ran system is controlled by a TBC GAP that could represent again the ancestral GAP architecture, prior to separation between Rab and Ran GTPases. That this could be reflective of the configuration in the last common eukaryotic ancestor is a tempting speculation.

Eukaryotic gene expression shares many ancestral properties, albeit with additionally species-specific proteins and novel pathways arising to address the specific evolutionary adaptations of each organism. Trypanosomes have sculpted their mRNA processing/export pathways in ways very distinct from opisthokonts, perhaps as a consequence of polycistronic transcription and PolI transcription of protein-encoding mRNAs. In trypanosomes, mRNA export and processing appear to be Ran-dependent, with no apparent Dbp5 or Gle1 homologs to drive export, another fundamental shift in how the pathway is controlled when compared with the canonical pathway in animals, fungi, plants, and most other lineages. Trypanosomes have generally provided evolutionary lessons in the plasticity of conserved eukaryotic machineries, given other examples of highly distinct seemingly kinetoplastid functions such as an atypical lamina, nuclear basket and divergent kinetochores. We anticipate that a more detailed dissection of the molecular players and mechanisms associated with these three Mex67 homologs will provide insights not only into the fascinating plasticity of their functionality but also into core principles of RNA processing and nuclear export mechanisms that must be shared between essentially all eukaryotes.

Acknowledgements

We are grateful to the Rockefeller University Genomics Resource Center (RRID:SCR_020986), especially Director Connie Zhao for all assistance with setting up and running our RNA-Seq experiments, Sebastian Hutchison (Quantum-Si), and Michele Tinti (University of Dundee) for advice on analysis of RNA-Seq data.

Author contributions: Samson O. Obado (Conceptualization [equal], Funding acquisition [equal], Investigation [equal], Methodology [equal], Project administration [equal], Supervision [equal], Writing—original draft [equal], Writing—review & editing [equal]), Peter C. Fridy (Data curation [equal], Formal analysis [equal], Methodology [equal], Writing—review & editing [equal]), Eva Hegedusova (Data curation [equal], Formal analysis [equal], Investigation [equal]), Trevor van Eeuwen (Formal analysis [equal], Methodology [equal]), Milana E. Stein (Investigation [equal]), Wenzhu Zhang (Formal analysis [equal]), Bryan Jensen (Investigation [supporting], Methodology [supporting]), Connor Chung (Formal analysis [equal], Investigation [equal], Methodology [equal]), Marc Brillantes (Investigation [equal]), Lucy Glover (Formal analysis [equal], Investigation [equal], Writing—review & editing [equal]), Zdenek Paris (Project administration [equal], Writing—review & editing [equal]), Brian T. Chait (Supervision [equal]), Mark Field (Conceptualization [equal], Supervision [equal]), and Michael Paul Rout (Conceptualization [equal], Supervision [equal])

Supplementary data

Supplementary data is available at NAR online.

Conflict of interest

None declared.

Funding

We are grateful to the Wellcome Trust (Investigator award 204697/Z/16/Z to M.C.F.), the National Institutes of Health (R01 AI140429-01A1 to M.P.R. and S.O., R21 AI096069, P41 GM109824, and R01 GM112108 to M.P.R.) and the National Science Foundation (Proposal No. 1818129 to S.O. and J.F-M) for financial support. This work was also supported by financial support by Institut pateur (to L.G.) and the Czech Science Foundation grants 20-11585S (to Z.P.) and 23-08669L (to Z.P.), and by the ERDF/ESF and MEYS CR projects: Centre for Research of Pathogenicity and Virulence of Parasites (CZ.02.1.01/0.0/0.0/16_019/0000759 to Z.P.) and RNA for Therapy (CZ.02.01.01/00/22_008/0004575 to

Z.P.). Funding to pay the Open Access publication charges for this article was provided by the National Institutes of Health [P41 GM109824, R01 AI140429-01A1, R01 GM112108, and R21 AI096069] and National Science Foundation [Proposal No. 1818129].

Data availability

Both processed and raw proteomic mass spectrometric (MS) data are available in the Zenodo database (https://zenodo.org/), which is a general-purpose open repository developed under the European OpenAIRE program and operated by CERN. The DOI associated with this publication is https://doi.org/10.5281/zenodo.8193998.

References

1. Daniel B, Nagy G, Nagy L. The intriguing complexities of mammalian gene regulation: how to link enhancers to regulated genes. Are we there yet? *FEBS Lett* 2014;588:2379–91. https://doi.org/10.1016/j.febslet.2014.05.041
2. Kaikkonen MU, Lam MT, Glass CK. Non-coding RNAs as regulators of gene expression and epigenetics. *Cardiovasc Res* 2011;90:430–40. https://doi.org/10.1093/cvr/cvr097
3. Shaul O. How introns enhance gene expression. *Int J Biochem Cell Biol* 2017;91:145–55. https://doi.org/10.1016/j.biocel.2017.06.016
4. Wu C. Chromatin remodeling and the control of gene expression. *J Biol Chem* 1997;272:28171–4. https://doi.org/10.1074/jbc.272.45.28171
5. Kramer S. Nuclear mRNA maturation and mRNA export control: from trypanosomes to opisthokonts. *Parasitology* 2021;148:1196–1218. https://doi.org/10.1017/S0031182021000068
6. Faraway R, Zenklusen D, Plaschka C. Mechanisms of messenger RNA packaging and export. *Annu Rev Cell Dev Biol* 2025;41:479–504. https://doi.org/10.1146/annurev-cellbio-101123-045256
7. Serpeloni M, Moraes CB, Muniz JR *et al.* An essential nuclear protein in trypanosomes is a component of mRNA transcription/export pathway. *PLoS One* 2011;6:e20730. https://doi.org/10.1371/journal.pone.0020730
8. Obado SO, Rout MP, Field MC. Sending the message: specialized RNA export mechanisms in trypanosomes. *Trends Parasitol* 2022;38:854–67. https://doi.org/10.1016/j.pt.2022.07.008
9. Makarov AA, Padilla-Mejia NE, Field MC. Evolution and diversification of the nuclear pore complex. *Biochem Soc Trans* 2021;49:1601–19. https://doi.org/10.1042/BST20200570
10. Inoue AH, Domingues PF, Serpeloni M *et al.* Proteomics uncovers novel components of an interactive protein network supporting RNA export in trypanosomes. *Mol Cell Proteomics* 2022;21:100208. https://doi.org/10.1016/j.mcpro.2022.100208
11. Okamura M, Inose H, Masuda S. RNA export through the NPC in eukaryotes. *Genes* 2015;6:124–49. https://doi.org/10.3390/genes6010124
12. Strambio-De-Castillia C, Niepel M, Rout MP. The nuclear pore complex: bridging nuclear transport and gene regulation. *Nat Rev Mol Cell Biol* 2010;11:490–501. https://doi.org/10.1038/nrm2928
13. Ashkenazy-Titelman A, Atrash MK, Boocholez A *et al.* RNA export through the nuclear pore complex is directional. *Nat Commun* 2022;13:5881. https://doi.org/10.1038/s41467-022-33572-7
14. Wing CE, Fung HYJ, Chook YM. Karyopherin-mediated nucleocytoplasmic transport. *Nat Rev Mol Cell Biol* 2022;23:307–28. https://doi.org/10.1038/s41580-021-00446-7
15. Santos-Rosa H, Moreno H, Simos G *et al.* Nuclear mRNA export requires complex formation between Mex67p and Mtr2p at the nuclear pores. *Mol Cell Biol* 1998;18:6826–38. https://doi.org/10.1128/MCB.18.11.6826
16. Wente SR, Rout MP. The nuclear pore complex and nuclear transport. *Cold Spring Harb Perspect Biol* 2010;2:a000562. https://doi.org/10.1101/cshperspect.a000562
17. Adams RL, Terry LJ, Wente SR. Nucleoporin FG domains facilitate mRNP remodeling at the cytoplasmic face of the nuclear pore complex. *Genetics* 2014;197:1213–24. https://doi.org/10.1534/genetics.114.164012
18. Alcazar-Roman AR, Tran EJ, Guo S *et al.* Inositol hexakisphosphate and Gle1 activate the DEAD-box protein Dbp5 for nuclear mRNA export. *Nat Cell Biol* 2006;8:711–6. https://doi.org/10.1038/ncb1427
19. Hodge CA, Colot HV, Stafford P *et al.* Rat8p/Dbp5p is a shuttling transport factor that interacts with Rat7p/Nup159p and Gle1p and suppresses the mRNA export defect of xpo1-1 cells. *EMBO J* 1999;18:5778–88. https://doi.org/10.1093/emboj/18.20.5778
20. Hodge CA, Tran EJ, Noble KN *et al.* The Dbp5 cycle at the nuclear pore complex during mRNA export I: dbp5 mutants with defects in RNA binding and ATP hydrolysis define key steps for Nup159 and Gle1. *Genes Dev* 2011;25:1052–64. https://doi.org/10.1101/gad.2041611
21. Montpetit B, Thomsen ND, Helmke KJ *et al.* A conserved mechanism of DEAD-box ATPase activation by nucleoporins and InsP6 in mRNA export. *Nature* 2011;472:238–42. https://doi.org/10.1038/nature09862
22. Noble KN, Tran EJ, Alcazar-Roman AR *et al.* The Dbp5 cycle at the nuclear pore complex during mRNA export II: nucleotide cycling and mRNP remodeling by Dbp5 are controlled by Nup159 and Gle1. *Genes Dev* 2011;25:1065–77. https://doi.org/10.1101/gad.2040611
23. Weirich CS, Erzberger JP, Berger JM *et al.* The N-terminal domain of Nup159 forms a beta-propeller that functions in mRNA export by tethering the helicase Dbp5 to the nuclear pore. *Mol Cell* 2004;16:749–60. https://doi.org/10.1016/j.molcel.2004.10.032
24. Weirich CS, Erzberger JP, Flick JS *et al.* Activation of the DExD/H-box protein Dbp5 by the nuclear-pore protein Gle1 and its coactivator InsP6 is required for mRNA export. *Nat Cell Biol* 2006;8:668–76. https://doi.org/10.1038/ncb1424
25. Katahira J, Strasser K, Podtelejnikov A *et al.* The Mex67p-mediated nuclear mRNA export pathway is conserved from yeast to human. *EMBO J* 1999;18:2593–609. https://doi.org/10.1093/emboj/18.9.2593
26. Adl SM, Simpson AG, Lane CE *et al.* The revised classification of eukaryotes. *J Eukaryotic Microbiol* 2012;59:429–514. https://doi.org/10.1111/j.1550-7408.2012.00644.x
27. Baldauf SL. The deep roots of eukaryotes. *Science* 2003;300:1703–6. https://doi.org/10.1126/science.1085544
28. Gabiatti BP, Krenzer J, Braune S *et al.* Detailed characterisation of the trypanosome nuclear pore architecture reveals conserved asymmetrical functional hubs that drive mRNA export. *PLoS Biol* 2025;23:e3003024. https://doi.org/10.1371/journal.pbio.3003024
29. Obado SO, Brillantes M, Uryu K *et al.* Interactome mapping reveals the evolutionary history of the nuclear pore complex. *PLoS Biol* 2016;14:e1002365, https://doi.org/10.1371/journal.pbio.1002365
30. Serpeloni M, Jimenez-Ruiz E, Vidal NM *et al.* UAP56 is a conserved crucial component of a divergent mRNA export pathway in *Toxoplasma gondii*. *Mol Microbiol* 2016;102:672–89, https://doi.org/10.1111/mmi.13485
31. Serpeloni M, Vidal NM, Goldenberg S *et al.* Comparative genomics of proteins involved in RNA nucleocytoplasmic export. *BMC Evol Biol* 2011;11:7. https://doi.org/10.1186/1471-2148-11-7

32. Berriman M, Ghedin E, Hertz-Fowler C *et al.* The genome of the African trypanosome *Trypanosoma brucei*. *Science* 2005;309:416–22. https://doi.org/10.1126/science.1112642
33. Cordon-Obras C, Gomez-Linan C, Torres-Rusillo S *et al.* Identification of sequence-specific promoters driving polycistronic transcription initiation by RNA polymerase II in trypanosomes. *Cell Rep* 2022;38:110221. https://doi.org/10.1016/j.celrep.2021.110221
34. Siegel TN, Hekstra DR, Kemp LE *et al.* Four histone variants mark the boundaries of polycistronic transcription units in *Trypanosoma brucei*. *Genes Dev* 2009;23:1063–76. https://doi.org/10.1101/gad.1790409
35. Clayton C. The regulation of trypanosome gene expression by RNA-binding proteins. *PLoS Pathog* 2013;9:e1003680. https://doi.org/10.1371/journal.ppat.1003680
36. Butterfield ER, Obado SO, Scutts SR *et al.* A lineage-specific protein network at the trypanosome nuclear envelope. *Nucleus* 2024;15:2310452. https://doi.org/10.1080/19491034.2024.2310452
37. Goos C, Dejung M, Wehman AM *et al.* Trypanosomes can initiate nuclear export co-transcriptionally. *Nucleic Acids Res* 2019;47:266–82. https://doi.org/10.1093/nar/gky1136
38. Dostalova A, Kaser S, Cristodero M *et al.* The nuclear mRNA export receptor Mex67–Mtr2 of *Trypanosoma brucei* contains a unique and essential zinc finger motif. *Mol Microbiol* 2013;88:728–39. https://doi.org/10.1111/mmi.12217
39. Kramer S, Kimblin NC, Carrington M. Genome-wide *in silico* screen for CCCH-type zinc finger proteins of *Trypanosoma brucei*, *Trypanosoma cruzi* and Leishmania major. *BMC Genomics* 2010;11:283. https://doi.org/10.1186/1471-2164-11-283
40. Schwede A, Manful T, Jha BA *et al.* The role of deadenylation in the degradation of unstable mRNAs in trypanosomes. *Nucleic Acids Res* 2009;37:5511–28. https://doi.org/10.1093/nar/gkp571
41. DeGrasse JA, DuBois KN, Devos D *et al.* Evidence for a shared nuclear pore complex architecture that is conserved from the last common eukaryotic ancestor. *Mol Cell Proteomics* 2009;8:2119–30. https://doi.org/10.1074/mcp.M900038-MCP200
42. O'Reilly AJ, Dacks JB, Field MC. Evolution of the karyopherin-beta family of nucleocytoplasmic transport factors; ancient origins and continued specialization. *PLoS One* 2011;6:e19308. https://doi.org/10.1371/journal.pone.0019308
43. Hegedusova E, Kulkarni S, Burgman B *et al.* The general mRNA exporters Mex67 and Mtr2 play distinct roles in nuclear export of tRNAs in trypanosoma brucei. *Nucleic Acids Res* 2019;47:8620–31. https://doi.org/10.1093/nar/gkz671
44. Buhlmann M, Walrad P, Rico E *et al.* NMD3 regulates both mRNA and rRNA nuclear export in African trypanosomes via an XPOI-linked pathway. *Nucleic Acids Res* 2015;43:4491–504. https://doi.org/10.1093/nar/gkv330
45. Rink C, Ciganda M, Williams N. The nuclear export receptors TbMex67 and TbMtr2 are required for ribosome biogenesis in *Trypanosoma brucei*. *mSphere* 2019;4:e00343–19. https://doi.org/10.1128/mSphere.00343-19
46. Chatterjee K, Majumder S, Wan Y *et al.* Sharing the load: Mex67–Mtr2 cofunctions with Los1 in primary tRNA nuclear export. *Genes Dev* 2017;31:2186–98. https://doi.org/10.1101/gad.305904.117
47. Faza MB, Chang Y, Occhipinti L *et al.* Role of Mex67–Mtr2 in the nuclear export of 40S pre-ribosomes. *PLoS Genet* 2012;8:e1002915. https://doi.org/10.1371/journal.pgen.1002915
48. Yao W, Lutzmann M, Hurt E. A versatile interaction platform on the Mex67–Mtr2 receptor creates an overlap between mRNA and ribosome export. *EMBO J* 2008;27:6–16. https://doi.org/10.1038/sj.emboj.7601947
49. Yao W, Roser D, Kohler A *et al.* Nuclear export of ribosomal 60S subunits by the general mRNA export receptor Mex67–Mtr2. *Mol Cell* 2007;26:51–62. https://doi.org/10.1016/j.molcel.2007.02.018
50. Senay C, Ferrari P, Rocher C *et al.* The Mtr2–Mex67 NTF2-like domain complex. Structural insights into a dual role of Mtr2 for yeast nuclear export. *J Biol Chem* 2003;278:48395–403. https://doi.org/10.1074/jbc.M308275200
51. Fribourg S, Braun IC, Izaurralde E *et al.* Structural basis for the recognition of a nucleoporin FG repeat by the NTF2-like domain of the TAP/p15 mRNA nuclear export factor. *Mol Cell* 2001;8:645–56. https://doi.org/10.1016/S1097-2765(01)00348-3
52. Fernandez-Martinez J, Kim SJ, Shi Y *et al.* Structure and function of the nuclear pore complex cytoplasmic mRNA export platform. *Cell* 2016;167:1215–28. https://doi.org/10.1016/j.cell.2016.10.028
53. Folkmann AW, Noble KN, Cole CN *et al.* Dbp5, Gle1-IP6 and Nup159: a working model for mRNP export. *Nucleus* 2011;2:540–8. https://doi.org/10.4161/nucl.2.6.17881
54. DuBois KN, Alsford S, Holden JM *et al.* NUP-1 is a large coiled-coil nucleoskeletal protein in trypanosomes with lamin-like functions. *PLoS Biol* 2012;10:e1001287. https://doi.org/10.1371/journal.pbio.1001287
55. Holden JM, Koreny L, Obado S *et al.* Nuclear pore complex evolution: a trypanosome Mlp analogue functions in chromosomal segregation but lacks transcriptional barrier activity. *MBoC* 2014;25:1421–36. https://doi.org/10.1091/mbc.e13-12-0750
56. Florini F, Naguleswaran A, Gharib WH *et al.* Unexpected diversity in eukaryotic transcription revealed by the retrotransposon hotspot family of trypanosoma brucei. *Nucleic Acids Res* 2019;47:1725–39. https://doi.org/10.1093/nar/gky1255
57. Kramer S. The ApaH-like phosphatase TbALPH1 is the major mRNA decapping enzyme of trypanosomes. *PLoS Pathog* 2017;13:e1006456. https://doi.org/10.1371/journal.ppat.1006456
58. Hirumi H, Hirumi K. Continuous cultivation of *Trypanosoma brucei* blood stream forms in a medium containing a low concentration of serum protein without feeder cell layers. *J Parasitol* 1989;75:985–9. https://doi.org/10.2307/3282883
59. Urbaniak MD, Martin DM, Ferguson MA. Global quantitative SILAC phosphoproteomics reveals differential phosphorylation is widespread between the procyclic and bloodstream form lifecycle stages of *Trypanosoma brucei*. *J Proteome Res* 2013;12:2233–44. https://doi.org/10.1021/pr400086y
60. Oberholzer M, Morand S, Kunz S *et al.* A vector series for rapid PCR-mediated C-terminal in situ tagging of *Trypanosoma brucei* genes. *Mol Biochem Parasitol* 2006;145:117–20. https://doi.org/10.1016/j.molbiopara.2005.09.002
61. Butterfield ER, Abbott JC, Field MC. Automated phylogenetic analysis using best reciprocal BLAST. *Methods Mol Biol* 2021;2369:41–63.
62. Edgar RC. Muscle5: high-accuracy alignment ensembles enable unbiased assessments of sequence homology and phylogeny. *Nat Commun* 2022;13:6968. https://doi.org/10.1038/s41467-022-34630-w
63. Lawrence TJ, Kauffman KT, Amrine KC *et al.* FAST: FAST analysis of sequences toolbox. *Front Genet* 2015;6:172. https://doi.org/10.3389/fgene.2015.00172
64. Price MN, Dehal PS, Arkin AP. FastTree 2–approximately maximum-likelihood trees for large alignments. *PLoS One* 2010;5:e9490. https://doi.org/10.1371/journal.pone.0009490
65. Obado SO, Field MC, Chait BT *et al.* High-efficiency isolation of nuclear envelope protein complexes from trypanosomes. *Methods Mol Biol* 2016;1411:67–80.
66. Fenyo D, Eriksson J, Beavis R. Mass spectrometric protein identification using the global proteome machine. *Methods Mol Biol* 2010;673:189–202.

67. Fridy PC, Li Y, Keegan S *et al.* A robust pipeline for rapid production of versatile nanobody repertoires. *Nat Methods* 2014;11:1253–60. https://doi.org/10.1038/nmeth.3170
68. Kohler A, Hurt E. Exporting RNA from the nucleus to the cytoplasm. *Nat Rev Mol Cell Biol* 2007;8:761–73. https://doi.org/10.1038/nrm2255
69. Kim D, Paggi JM, Park C *et al.* Graph-based genome alignment and genotyping with HISAT2 and HISAT-genotype. *Nat Biotechnol* 2019;37:907–15. https://doi.org/10.1038/s41587-019-0201-4
70. Liao Y, Smyth GK, Shi W. featureCounts: an efficient general purpose program for assigning sequence reads to genomic features. *Bioinformatics* 2014;30:923–30. https://doi.org/10.1093/bioinformatics/btt656
71. Robinson MD, McCarthy DJ, Smyth GK. edgeR: a bioconductor package for differential expression analysis of digital gene expression data. *Bioinformatics* 2010;26:139–40. https://doi.org/10.1093/bioinformatics/btp616
72. Alsford S, Turner DJ, Obado SO *et al.* High-throughput phenotyping using parallel sequencing of RNA interference targets in the African trypanosome. *Genome Res* 2011;21:915–24. https://doi.org/10.1101/gr.115089.110
73. Wirtz E, Leal S, Ochatt C *et al.* A tightly regulated inducible expression system for conditional gene knock-outs and dominant-negative genetics in Trypanosoma brucei. *Mol Biochem Parasitol* 1999;99:89–101. https://doi.org/10.1016/S0166-6851(99)00002-X
74. Soding J, Biegert A, Lupas AN. The HHpred interactive server for protein homology detection and structure prediction. *Nucleic Acids Res* 2005;33:W244–8. https://doi.org/10.1093/nar/gki408
75. Jumper J, Evans R, Pritzel A *et al.* Highly accurate protein structure prediction with AlphaFold. *Nature* 2021;596:583–9. https://doi.org/10.1038/s41586-021-03819-2
76. Wheeler RJ. A resource for improved predictions of Trypanosoma and Leishmania protein three-dimensional structure. *PLoS One* 2021;16:e0259871. https://doi.org/10.1371/journal.pone.0259871
77. Pettersen EF, Goddard TD, Huang CC *et al.* UCSF ChimeraX: structure visualization for researchers, educators, and developers. *Protein Sci* 2021;30:70–82. https://doi.org/10.1002/pro.3943
78. Gabernet-Castello C, O'Reilly AJ, Dacks JB *et al.* Evolution of Tre-2/Bub2/Cdc16 (TBC) Rab GTPase-activating proteins. *MBoC* 2013;24:1574–83. https://doi.org/10.1091/mbc.e12-07-0557
79. Seewald MJ, Korner C, Wittinghofer A *et al.* RanGAP mediates GTP hydrolysis without an arginine finger. *Nature* 2002;415:662–6. https://doi.org/10.1038/415662a
80. Herold A, Suyama M, Rodrigues JP *et al.* TAP (NXF1) belongs to a multigene family of putative RNA export factors with a conserved modular architecture. *Mol Cell Biol* 2000;20:8996–9008. https://doi.org/10.1128/MCB.20.23.8996-9008.2000
81. Segref A, Sharma K, Doye V *et al.* Mex67p, a novel factor for nuclear mRNA export, binds to both poly(A)+ RNA and nuclear pores. *EMBO J* 1997;16:3256–71. https://doi.org/10.1093/emboj/16.11.3256
82. Rink C, Williams N. Unique interactions of the nuclear export receptors TbMex67 and TbMtr2 with components of the 5S ribonuclear particle in trypanosoma brucei. *mSphere* 2019;4:e00471–19. https://doi.org/10.1128/mSphere.00471-19
83. Gwizdek C, Iglesias N, Rodriguez MS *et al.* Ubiquitin-associated domain of Mex67 synchronizes recruitment of the mRNA export machinery with transcription. *Proc Natl Acad Sci USA* 2006;103:16376–81. https://doi.org/10.1073/pnas.0607941103
84. Aibara S, Katahira J, Valkov E *et al.* The principal mRNA nuclear export factor NXF1:NXT1 forms a symmetric binding platform that facilitates export of retroviral CTE-RNA. *Nucleic Acids Res* 2015;43:1883–93. https://doi.org/10.1093/nar/gkv032
85. Blevins MB, Smith AM, Phillips EM *et al.* Complex formation among the RNA export proteins Nup98, Rae1/Gle2, and TAP. *J Biol Chem* 2003;278:20979–88. https://doi.org/10.1074/jbc.M302061200
86. Murphy R, Watkins JL, Wente SR. GLE2, a *Saccharomyces cerevisiae* homologue of the *Schizosaccharomyces pombe* export factor RAE1, is required for nuclear pore complex structure and function. *MBoC* 1996;7:1921–37. https://doi.org/10.1091/mbc.7.12.1921
87. Pritchard CE, Fornerod M, Kasper LH *et al.* RAE1 is a shuttling mRNA export factor that binds to a GLEBS-like NUP98 motif at the nuclear pore complex through multiple domains. *J Cell Biol* 1999;145:237–54. https://doi.org/10.1083/jcb.145.2.237
88. Kramer S, Bannerman-Chukualim B, Ellis L *et al.* Differential localization of the two *T. brucei* poly(A) binding proteins to the nucleus and RNP granules suggests binding to distinct mRNA pools. *PLoS One* 2013;8:e54004. https://doi.org/10.1371/journal.pone.0054004
89. Zoltner M, Krienitz N, Field MC *et al.* Comparative proteomics of the two *T. brucei* PABPs suggests that PABP2 controls bulk mRNA. *PLoS Negl Trop Dis* 2018;12:e0006679. https://doi.org/10.1371/journal.pntd.0006679
90. Natalizio BJ, Wente SR. Postage for the messenger: designating routes for nuclear mRNA export. *Trends Cell Biol* 2013;23:365–73. https://doi.org/10.1016/j.tcb.2013.03.006
91. Bishola Tshitenge T, Clayton C. The *Trypanosoma brucei* RNA-binding protein DRBD18 ensures correct mRNA *trans*-splicing and polyadenylation patterns. *RNA* 2022;28:1239–62. https://doi.org/10.1261/rna.079258.122
92. Mishra A, Kaur JN, McSkimming DI *et al.* Selective nuclear export of mRNAs is promoted by DRBD18 in *Trypanosoma brucei*. *Mol Microbiol* 2021;116:827–40. https://doi.org/10.1111/mmi.14773
93. Dean S, Sunter JD, Wheeler RJ. TrypTag.org: a trypanosome genome-wide protein localisation resource. *Trends Parasitol* 2017;33:80–2. https://doi.org/10.1016/j.pt.2016.10.009
94. Klingauf-Nerurkar P, Gillet LC, Portugal-Calisto D *et al.* The GTPase Nog1 co-ordinates the assembly, maturation and quality control of distant ribosomal functional centers. *eLife* 2020;9 :e52474. https://doi.org/10.7554/eLife.52474
95. Pestov DG, Stockelman MG, Strezoska Z *et al.* ERB1, the yeast homolog of mammalian Bop1, is an essential gene required for maturation of the 25S and 5.8S ribosomal RNAs. *Nucleic Acids Res* 2001;29:3621–30. https://doi.org/10.1093/nar/29.17.3621
96. Grant RP, Neuhaus D, Stewart M. Structural basis for the interaction between the Tap/NXF1 UBA domain and FG nucleoporins at 1A resolution. *J Mol Biol* 2003;326:849–58. https://doi.org/10.1016/S0022-2836(02)01474-2
97. Suyama M, Doerks T, Braun IC *et al.* Prediction of structural domains of TAP reveals details of its interaction with p15 and nucleoporins. *EMBO Rep* 2000;1:53–8. https://doi.org/10.1093/embo-reports/kvd009
98. Kent HM, Moore MS, Quimby BB *et al.* Engineered mutants in the switch II loop of Ran define the contribution made by key residues to the interaction with nuclear transport factor 2 (NTF2) and the role of this interaction in nuclear protein import. *J Mol Biol* 1999;289:565–77. https://doi.org/10.1006/jmbi.1999.2775
99. Sarkar A, Pech M, Thoms M *et al.* Ribosome-stalk biogenesis is coupled with recruitment of nuclear-export factor to the nascent 60S subunit. *Nat Struct Mol Biol* 2016;23:1074–82. https://doi.org/10(?PMU?)1038/nsmb.3312
100. Jensen BC, Wang Q, Kifer CT *et al.* The NOG1 GTP-binding protein is required for biogenesis of the 60 S ribosomal subunit. *J Biol Chem* 2003;278:32204–11. https://doi.org/10.1074/jbc.M304198200
101. Lueong S, Merce C, Fischer B *et al.* Gene expression regulatory networks in *Trypanosoma brucei*: insights into the role of the mRNA-binding proteome. *Mol Microbiol* 2016;100:457–71. https://doi.org/10.1111/mmi.13328
102. Hendriks EF, Robinson DR, Hinkins M *et al.* A novel CCCH protein which modulates differentiation of *Trypanosoma brucei*

to its procyclic form. *EMBO J* 2001;20:6700–11. https://doi.org/10.1093/emboj/20.23.6700
103. Shi H, Butler K, Tschudi C. A single-point mutation in the RNA-binding protein 6 generates *Trypanosoma brucei* metacyclics that are able to progress to bloodstream forms *in vitro*. *Mol Biochem Parasitol* 2018;224:50–6. https://doi.org/10.1016/j.molbiopara.2018.07.011
104. Kolev NG, Ramey-Butler K, Cross GA *et al.* Developmental progression to infectivity in *Trypanosoma brucei* triggered by an RNA-binding protein. *Science* 2012;338:1352–3. https://doi.org/10.1126/science.1229641
105. Mony BM, MacGregor P, Ivens A *et al.* Genome-wide dissection of the quorum sensing signalling pathway in *Trypanosoma brucei*. *Nature* 2014;505:681–5. https://doi.org/10.1038/nature12864
106. Richardson JP, Beecroft RP, Tolson DL *et al.* Procyclin: an unusual immunodominant glycoprotein surface antigen from the procyclic stage of African trypanosomes. *Mol Biochem Parasitol* 1988;31:203–16. https://doi.org/10.1016/0166-6851(88)90150-8
107. Colmerauer ME, Davis CE, Pearson TW. The trypanosome surface glycoprotein procyclin is expressed only on tsetse fly vector stages of the parasite. *Parasitol Res* 1989;76:171–3. https://doi.org/10.1007/BF00930841
108. Roditi I, Schwarz H, Pearson TW *et al.* Procyclin gene expression and loss of the variant surface glycoprotein during differentiation of trypanosoma brucei. *J Cell Biol* 1989;108:737–46. https://doi.org/10.1083/jcb.108.2.737
109. Hoeijmakers JH, Frasch AC, Bernards A *et al.* Novel expression-linked copies of the genes for variant surface antigens in trypanosomes. *Nature* 1980;284:78–80. https://doi.org/10.1038/284078a0
110. Boothroyd JC, Cross GA, Hoeijmakers JH. *et al.* A variant surface glycoprotein of *Trypanosoma brucei* synthesized with a C-terminal hydrophobic 'tail' absent from purified glycoprotein. *Nature* 1980;288:624–6. https://doi.org/10.1038/288624a0
111. Gunzl A, Bruderer T, Laufer G *et al.* RNA polymerase I transcribes procyclin genes and variant surface glycoprotein gene expression sites in *Trypanosoma brucei*. *Euk Cell* 2003;2:542–51. https://doi.org/10.1128/EC.2.3.542-551.2003
112. Lee MG, Van der Ploeg LH. Transcription of protein-coding genes in trypanosomes by RNA polymerase I. *Annu Rev Microbiol* 1997;51:463–89. https://doi.org/10.1146/annurev.micro.51.1.463
113. Vanhamme L, Poelvoorde P, Pays A *et al.* Differential RNA elongation controls the variant surface glycoprotein gene expression sites of *Trypanosoma brucei*. *Mol Microbiol* 2000;36:328–40. https://doi.org/10.1046/j.1365-2958.2000.01844.x
114. Kassem A, Pays E, Vanhamme L. Transcription is initiated on silent variant surface glycoprotein expression sites despite monoallelic expression in *Trypanosoma brucei*. *Proc Natl Acad Sci USA* 2014;111:8943–8. https://doi.org/10.1073/pnas.1404873111
115. Faria J, Briggs EM, Black JA *et al.* Emergence and adaptation of the cellular machinery directing antigenic variation in the African trypanosome. *Curr Opin Microbiol* 2022;70:102209. https://doi.org/10.1016/j.mib.2022.102209
116. Pozzi B, Naguleswaran A, Florini F *et al.* The RNA export factor TbMex67 connects transcription and RNA export in *Trypanosoma brucei* and sets boundaries for RNA polymerase I. *Nucleic Acids Res* 2023;51:5177–92. https://doi.org/10.1093/nar/gkad251
117. Galvan SC, Castro C, Segura E *et al.* Nucleotide sequences of the six very small molecules of *Trypanosoma cruzi* ribosomal RNA. *Nucl Acids Res* 1991;19:2496. https://doi.org/10.1093/nar/19.9.2496
118. Vanden Broeck A, Klinge S. Eukaryotic ribosome assembly. *Annu Rev Biochem* 2024;93:189–210. https://doi.org/10.1146/annurev-biochem-030222-113611
119. Rajan KS, Chikne V, Decker K *et al.* Unique aspects of rRNA biogenesis in trypanosomatids. *Trends Parasitol* 2019;35:778–94. https://doi.org/10.1016/j.pt.2019.07.012
120. Hobeika M, Brockmann C, Gruessing F *et al.* Structural requirements for the ubiquitin-associated domain of the mRNA export factor Mex67 to bind its specific targets, the transcription elongation THO complex component Hpr1 and nucleoporin FXFG repeats. *J Biol Chem* 2009;284:17575–83. https://doi.org/10.1074/jbc.M109.004374
121. Brown JA, Bharathi A, Ghosh A *et al.* A mutation in the *Schizosaccharomyces pombe* rae1 gene causes defects in poly(A)+ RNA export and in the cytoskeleton. *J Biol Chem* 1995;270:7411–9. https://doi.org/10.1074/jbc.270.13.7411
122. Izaurralde E. A novel family of nuclear transport receptors mediates the export of messenger RNA to the cytoplasm. *Eur J Cell Biol* 2002;81:577–84. https://doi.org/10.1078/0171-9335-00273
123. Jun L, Frints S, Duhamel H *et al.* NXF5, a novel member of the nuclear RNA export factor family, is lost in a male patient with a syndromic form of mental retardation. *Curr Biol* 2001;11:1381–91. https://doi.org/10.1016/S0960-9822(01)00419-5
124. Kerkow DE, Carmel AB, Menichelli E *et al.* The structure of the NXF2/NXT1 heterodimeric complex reveals the combined specificity and versatility of the NTF2-like fold. *J Mol Biol* 2012;415:649–65. https://doi.org/10.1016/j.jmb.2011.11.027
125. Yang J, Bogerd HP, Wang PJ *et al.* Two closely related human nuclear export factors utilize entirely distinct export pathways. *Mol Cell* 2001;8:397–406. https://doi.org/10.1016/S1097-2765(01)00303-3
126. Lai D, Sakkas D, Huang Y. The fragile X mental retardation protein interacts with a distinct mRNA nuclear export factor NXF2. *RNA* 2006;12:1446–9. https://doi.org/10.1261/rna.94306
127. Zhang M, Wang Q, Huang Y. Fragile X mental retardation protein FMRP and the RNA export factor NXF2 associate with and destabilize Nxf1 mRNA in neuronal cells. *Proc Natl Acad Sci USA* 2007;104:10057–62. https://doi.org/10.1073/pnas.0700169104
128. Alber F, Dokudovskaya S, Veenhoff LM *et al.* The molecular architecture of the nuclear pore complex. *Nature* 2007;450:695–701. https://doi.org/10.1038/nature06405
129. Katahira J, Miki T, Takano K *et al.* Nuclear RNA export factor 7 is localized in processing bodies and neuronal RNA granules through interactions with shuttling hnRNPs. *Nucleic Acids Res* 2008;36:616–28. https://doi.org/10.1093/nar/gkm556
130. Vanmarsenille L, Verbeeck J, Belet S *et al.* Generation and characterization of an Nxf7 knockout mouse to study NXF5 deficiency in a patient with intellectual disability. *PLoS One* 2013;8:e64144. https://doi.org/10.1371/journal.pone.0064144
131. Tan W, Zolotukhin AS, Tretyakova I *et al.* Identification and characterization of the mouse nuclear export factor (Nxf) family members. *Nucleic Acids Res* 2005;33:3855–65. https://doi.org/10.1093/nar/gki706
132. Wiegand HL, Coburn GA, Zeng Y *et al.* Formation of Tap/NXT1 heterodimers activates Tap-dependent nuclear mRNA export by enhancing recruitment to nuclear pore complexes. *Mol Cell Biol* 2002;22:245–56. https://doi.org/10.1128/MCB.22.1.245-256.2002
133. Maishman L, Obado SO, Alsford S *et al.* Co-dependence between trypanosome nuclear lamina components in nuclear stability and control of gene expression. *Nucleic Acids Res* 2016;44:10554–70. https://doi.org/10.1093/nar/gkw751

Received: August 7, 2023. **Revised:** November 24, 2025. **Accepted:** November 25, 2025